Magmatism in the Bransfield Basin: Rifting of the South Shetland Arc?

Susanne Fretzdorff,[1] Tim J. Worthington,[1] Karsten M. Haase,[1] Roger Hékinian,[1] Leander Franz,[2] Randall A. Keller,[3] and Peter Stoffers[1]

Received 26 February 2004; revised 5 August 2004; accepted 20 August 2004; published 14 December 2004.

[1] Bransfield Basin is an actively extending marginal basin separating the inactive South Shetland arc from the northern Antarctic Peninsula. Rift-related volcanism is widespread throughout the central Bransfield Basin, but the wider eastern Bransfield Basin was previously unsampled. Lavas recovered from the eastern subbasin form three distinct groups: (1) Bransfield Group has moderate large-ion lithophile element (LILE) enrichment relative to normal mid-ocean ridge basalt (NMORB), (2) Gibbs Group has strong LILE enrichment and is restricted to a relic seamount interpreted as part of the South Shetland arc, and (3) fresh alkali basalt was recovered from the NE part of the basin near Spanish Rise. The subduction-related component in Bransfield and Gibbs Group lavas is a LILE-rich fluid with radiogenic Sr, Nd, and Pb isotope compositions derived predominantly from subducting sediment. These lavas can be modeled as melts from Pacific MORB source mantle contaminated by up to 5% of the subduction-related component. They further reveal that Pacific mantle, rather than South Atlantic mantle, has underlain Bransfield Basin since 3 Ma. Magma productivity decreases abruptly east of Bridgeman Rise, and lavas with the least subduction component outcrop at that end. Both the eastward decrease in subduction component and occurrence of young alkali basalts require that subduction-modified mantle generated during the lifetime of the South Shetland arc has been progressively removed from NE to SW. This is inconsistent with previous models suggesting continued slow subduction at the South Shetland Trench but instead favors models in which the South Scotia Ridge fault has propagated westward since 3 Ma generating transtension across the basin. *INDEX TERMS:* 1040 Geochemistry: Isotopic composition/chemistry; 3640 Mineralogy and Petrology: Igneous petrology; 3655 Mineralogy and Petrology: Major element composition; 3670 Mineralogy and Petrology: Minor and trace element composition; *KEYWORDS:* Bransfield Basin, back-arc basin, volcanic arc, geochemistry

Citation: Fretzdorff, S., T. J. Worthington, K. M. Haase, R. Hékinian, L. Franz, R. A. Keller, and P. Stoffers (2004), Magmatism in the Bransfield Basin: Rifting of the South Shetland Arc?, *J. Geophys. Res.*, *109*, B12208, doi:10.1029/2004JB003046.

1. Introduction

[2] Back-arc basins develop behind active subduction-related volcanic arcs and display a wide range of tectonic and magmatic styles that are functions of the opening mechanisms, lithospheric structure and composition, and interplay of mantle sources with subduction-related components [*Hawkins*, 1995; *Pearce et al.*, 1995; *Parson and Wright*, 1996; *Gribble et al.*, 1998; *Sinton et al.*, 2003; *Martinez and Taylor*, 2003; *Taylor and Martinez*, 2003]. Extension in back-arc basins is generally attributed to mantle convection induced either directly by the subducting slab or via trench roll-back. However, the transition between an initial phase of crustal rifting (localized volcanism) to subsequent seafloor spreading (oceanic crust generation) is complex and involves a reorganization of mantle convection from lateral flow beneath rifts to upwelling beneath mature spreading axes together with commensurate changes in geochemistry that reflect a greater slab-derived (hydrous) component during near-arc rifting [*Gribble et al.*, 1998]. Furthermore, controversy has surrounded the geochemical characteristics of lavas erupted during the rifting stage. It has been argued that this back-arc basin basalt (BABB) constitutes a major lava type with a distinctive composition between that of mid-ocean ridge basalt (MORB) and arc basalt [*Fryer et al.*, 1990], whereas others consider BABB to be a continuum of compositions that evolve from relatively arc-like during rifting to MORB-like during seafloor spreading as the distance between the extension axis and volcanic arc increases [*Stern et al.*, 1990; *Pearce et al.*, 1995]. In the latter model, changes in BABB geochemistry may yield insights into the composition of the material flux derived from the subducting slab at different depths.

[1]Institut für Geowissenschaften, Abteilung Geochemie, Christian-Albrechts-Universität zu Kiel, Kiel, Germany.
[2]Institut für Mineralogie, Technische Universität Bergakademie Freiberg, Freiberg, Germany.
[3]College of Oceanic and Atmospheric Sciences, Oregon State University, Corvallis, Oregon, USA.

0148-0227/04/2004JB003046$09.00

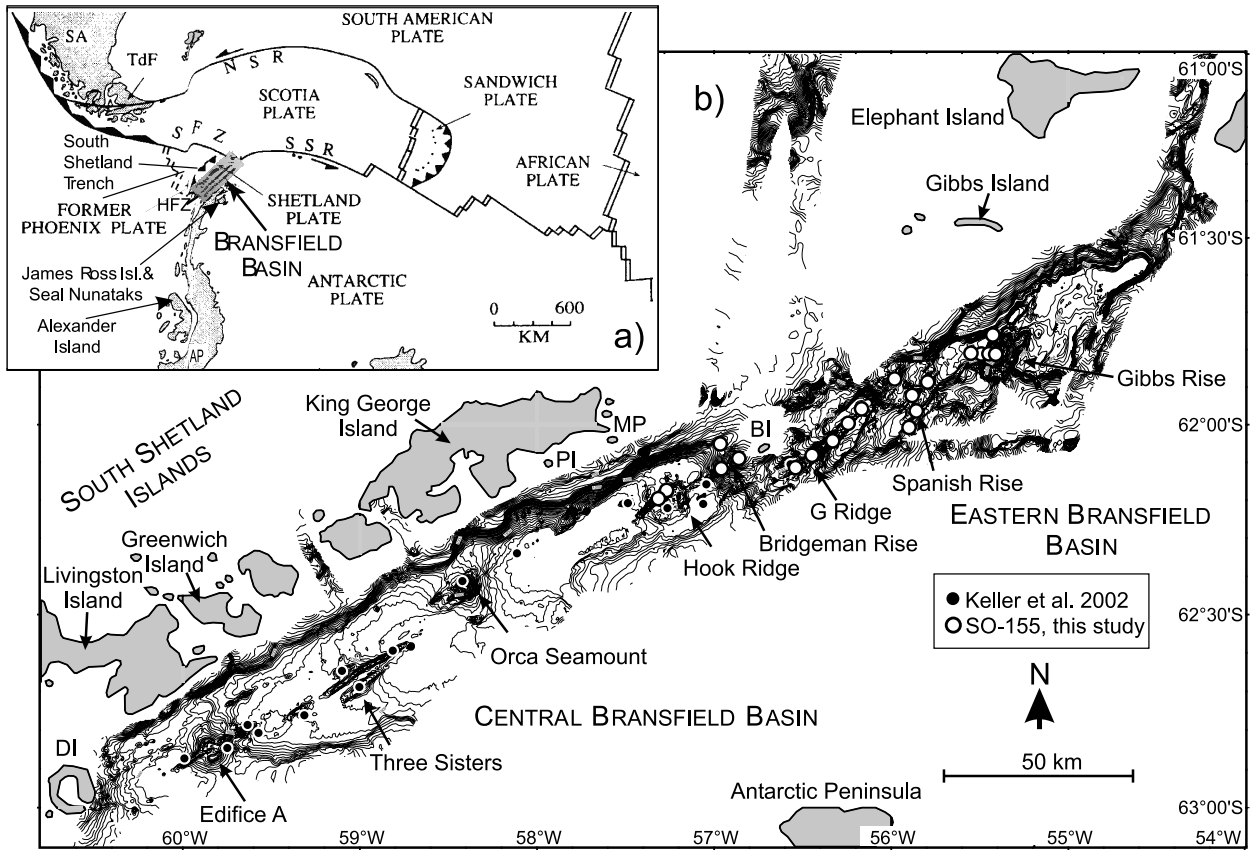

Figure 1. (a) Tectonic setting of the Bransfield Basin, Antarctica [after *Klepeis and Lawver*, 1996]. Abbreviations are SA, South America; TdF, Tierra del Fuego; AP, Antarctic Peninsula; HFZ, Hero Fracture Zone; SFZ, Shackleton Fracture Zone; SSR, South Scotia Ridge; and NSR, North Scotia Ridge. (b) Bathymetry of the central and eastern Bransfield Basin (100 m contours after *Lawver et al.* [1996] and G. P. Klinkhammer (unpublished bathymetric data, 1999), with sampling stations from SO-155 and *Keller et al.* [2002]. Edifice A, Three Sisters, Orca Seamount, and Hook Ridge are named by *González-Ferrán* [1991], *Lawver et al.* [1996], *Gràcia et al.* [1996], and *Klinkhammer et al.* [2001]. Here, we name Bridgeman Rise after the nearby Bridgeman Island, G Ridge from Edifice G of *Gràcia et al.* [1996], Spanish Rise after recent Spanish geophysical surveys of the eastern Bransfield Basin [e.g., *Gràcia et al.*, 1996, 1997], and Gibbs Rise from proximity to Gibbs Island. Abbreviations are DI, Deception Island; PI, Penguin Island; MP, Melville Peak; BI, Bridgeman Island.

[3] Previous studies of BABB have focused on the active back-arc basins of the western Pacific and the southern Atlantic [*Hawkins*, 1995; *Gribble et al.*, 1998; *Leat et al.*, 2000; *Peate et al.*, 2001; *Fretzdorff et al.*, 2002; *Martinez and Taylor*, 2003; *Sinton et al.*, 2003]. Less well known is the tectonic regime and composition of lavas in the Bransfield Basin, located behind the South Shetland arc on the Antarctic Peninsula (Figure 1). A model invoking incipient seafloor spreading with focused volcanism in the central Bransfield Basin grading to crustal rifting in the eastern Bransfield Basin has been proposed from geophysical studies [*Gràcia et al.*, 1996]. Lavas closely resembling enriched MORB (EMORB) outcrop in the middle of the central Bransfield Basin, but other nearby lavas have arc-like compositions and there are no systematic changes in lava geochemistry along the central Bransfield Basin axis [*Keller et al.*, 2002]. To gain new insights into magma genesis beneath the Bransfield Basin, we collected a series of lavas from the previously unsampled eastern Bransfield Basin during early 2001 [*Herzig and Party of SO-155*, 2001]. Geochemical and isotopic analyses of these lavas allow us to examine changes in magma genesis and mantle sources throughout the central and eastern Bransfield Basin, as well as yielding new insights into the development of this atypical volcanically active basin.

2. Bransfield Basin

2.1. Tectonic Setting and Volcanism

[4] Subduction of the Phoenix Plate beneath the continental crust of the Antarctic Peninsula at the South Shetland Trench commenced during the Mesozoic [*Barker*, 1982; *Barker et al.*, 1991]. The Antarctic–Phoenix spreading axis was cut by a series of NNW–SSE trending fracture zones whose ridge segments were progressively eliminated from SW to NE during a series of ridge–trench collisions between 54 and 3 Ma [*Larter and Barker*, 1991]. Seafloor magnetization indicates that spreading on the last three ridge

segments terminated at 3.3 Ma, and this probably coincided with elimination of the ridge segment SW of the Hero Fracture Zone [*Barker*, 1982; *Larter and Barker*, 1991; *Livermore et al.*, 2000]. Magmatism associated with Phoenix Plate subduction built a volcanic arc composed of low-K to medium-K series lavas along the Antarctic Peninsula and extending through the South Shetland Islands [*Pankhurst and Smellie*, 1983; *Smellie et al.*, 1984; *Birkenmajer et al.*, 1986]. Pulses of arc volcanism at 130–110, 90–70, 60–40, and 30–20 Ma are suggested by the clustering of dated lavas. Excluding Bransfield Basin, post-20 Ma lavas are restricted to a few outcrops on Livingston and Greenwich Islands [*Smellie et al.*, 1984]. Their paucity may be a consequence of subducting young oceanic crust [*Keller et al.*, 1991], or alternatively, the post-20 Ma arc may have subsided beneath sea level as Bransfield Basin opened. Sparse outcrops of alkali basalt, similar in composition to ocean island basalt (OIB) and ranging in age from 15 to <0.1 Ma, also occur on James Ross Island, Seal Nunataks and Alexander Island (Figure 1) [*Hole*, 1988; *Smellie et al.*, 1988; *Hole et al.*, 1993, 1995; *Lawver et al.*, 1995].

[5] Bransfield Basin is a 400-km-long, 60-km-wide, marginal basin comprising three subbasins that separate the South Shetland Islands from the Antarctic Peninsula (Figure 1). The western Bransfield Basin consists of crustal blocks downfaulted by ~1 km and is amagmatic [*Barker and Austin*, 1998]. In contrast, the central Bransfield Basin is deeper (to 1950 m), bounded by the large Quaternary Deception Island and Bridgeman Island volcanoes, and characterized by a series of semiregularly spaced submarine volcanoes that delineate the boundaries of flat-floored, thickly sedimented, bathymetric steps that deepen toward the NE [*Gràcia et al.*, 1996; *Prieto et al.*, 1999]. The eastern Bransfield Basin consists of four lozenge-shaped troughs up to 2750 m deep, and its rough seafloor has been interpreted as a series of widely scattered small volcanic cones [*Gràcia et al.*, 1996]. Crustal thickness beneath the central Bransfield Basin axis increases toward the SW from 10 to 15 km, consistent with SW directed rift propagation, and also thickens with distance from the basin axis attaining 20–26 km beneath the South Shetland Islands and 14–20 km at the Antarctic Peninsula margin [*Barker et al.*, 2003; *Christeson et al.*, 2003]. The main phase of basin development probably began when crustal accretion ceased at the Antarctic-Phoenix spreading axis [*Barker et al.*, 1991], although it has been suggested that an existing marginal basin was reactivated at that time [*Gambôa and Maldonado*, 1990]. Geodetic measurements utilizing GPS indicate present-day extension at ~10 mm/yr orthogonal to the basin axis [*Dietrich et al.*, 2001].

[6] Widespread volcanism developed within Bransfield Basin during the Quaternary, building a now eroded subaerial edifice (Melville Peak) and a small cinder cone (Penguin Island) along the northern basin margin together with a series of predominantly submarine volcanoes along the axis of the central Bransfield Basin (including Deception and Bridgeman Islands; Figure 1). Many of these seamounts have the morphology of a cone bisected by a highstanding volcanic ridge, with the youngest volcanism concentrated along the ridge axis [*Gràcia et al.*, 1996]. These ridges parallel the basin margins (N55–60°), but form a series of discontinuous and offset lineaments. Fresh glassy lavas ranging from arc-like to resembling EMORB in composition, and spanning the range from basalt to trachyte, have been dredged from these seamounts [*Fisk*, 1990; *Keller et al.*, 1991, 2002]. The most arc-like lavas, as determined by generally higher ratios of the large-ion lithophile elements (LILE) to high field strength elements (HFSE) and more radiogenic $^{87}Sr/^{86}Sr$ compositions, outcrop at the NE end of the subbasin, whereas those most resembling EMORB occur in the middle. Nevertheless, the LILE do not behave as a coherent group. Some volcanic centers are enriched in particular LILE and not in others relative to the HFSE, and there are no systematic changes in lava composition along the central Bransfield Basin [*Keller et al.*, 2002]. Hydrothermal venting takes place near the summit of several volcanoes [*Dählmann et al.*, 2001; *Klinkhammer et al.*, 2001; *Somoza et al.*, 2004].

2.2. Station Locations and Haul Descriptions

[7] Lavas were recovered using either a dredge or video-controlled grab from 23 stations in the Bransfield Basin during the HYDROARC (SO-155) cruise of the FS *Sonne* in February–March 2001 [*Herzig and Party of SO-155*, 2001]. The stations were located on five major structures spaced at ~25 km intervals (Figure 1): (1) Hook Ridge is an elongated hydrothermally active volcano in the NE part of the central Bransfield Basin, (2) Bridgeman Rise is a complex region separating the central and eastern Bransfield Basins that features two highstanding volcanic constructs (Bridgeman Island in the east, an unnamed edifice in the west) and is flanked to the north and south by basin-parallel valleys, (3) G Ridge is a prominent 30-km-long basin-parallel ridge extending from the crest of the southern valley on Bridgeman Rise into a 2-km-deep trough, (4) Spanish Rise is a highstanding region flanked to the north and south by basin-parallel valleys, and (5) Gibbs Rise has the form of a large conical seamount whose NW flank is terminated by a near-vertical escarpment interpreted as a fault. Ice-rafted erratics were recovered at most stations. The principal erratic lithologies were finely laminated biotite schists, coarse-grained plutonic rocks (gabbros, diorites and granites), and quartz-veined sediments (shale, greywacke and quartz wacke). Each of these lithologies outcrops on the nearby South Shetland Islands. Most dredge hauls contained no more than three distinct lava populations despite ground tracks of ~500 m, and all lavas were carefully examined for evidence of rounding or weathering in order to exclude possible erratics.

[8] Lavas from Hook Ridge were exclusively fresh glassy dacite. At Bridgeman Rise, fresh glassy lavas were recovered from the lower flanks of the western ridge whereas a more weathered sequence of sparsely olivine- and plagioclase-bearing lavas were recovered from the higher stations. Fresh glassy basalt, locally plagioclase-bearing, was also recovered from the northern valley of Bridgeman Rise. Lavas from G Ridge ranged from aphyric to sparsely olivine and plagioclase bearing, and from fresh (at the highest and second to lowest of 5 stations) to weakly weathered with palagonized rims and clay-filled vesicles. The proportion of weathered lavas on G Ridge, and their degree of weathering, is far greater than at the stations farther SW and indicates that much of G Ridge has not been resurfaced in recent times. Stations on Spanish Rise recovered weakly to mod-

erately weathered lavas, often with palagonized crusts and sparsely olivine bearing. However, fresh lavas were restricted to one station in the southern valley of Spanish Rise. Lavas were recovered from Gibbs Rise by dredging up the steep north facing scarp, and consisted of moderately to deeply weathered, strongly porphyritic, plagioclase-bearing andesite and dolerite. Hydrothermal alteration was widespread, and most blocks consisted of strongly chloritized or silicified variants, commonly with disseminated pyrite and other sulfides. Attempts to recover material from small (~200 m high) bathymetric anomalies in the deeper parts of the eastern Bransfield Basin near Gibbs Rise only obtained compacted sediments and glacial erratics.

3. Analytical Techniques

[9] Cores composing the freshest material were cut from 71 lavas, coarse crushed, washed thoroughly in deionized water to remove possible contamination by seawater salts, and then crushed to a fine powder in an agate mortar. For major element determinations, 0.6 grams of powder was mixed with lithium tetraborate and ammonium nitrate, fused to a homogeneous glass bead, and analyzed using a Philips PW1400 XRF spectrometer (Universität Kiel) equipped with a Rh tube and calibrated against international rock standards (Table 1; major element compositions for samples not subsequently analyzed for trace elements are presented in the auxiliary material[1]). Precision (2σ) for most major elements was better than 1%, with exceptions being TiO_2, Na_2O and P_2O_5 (~5%), and accuracy relative to BHVO-1 was better than 1%. Loss on ignition was determined by weight loss of 3 g of powder heated to 1000°C for 2 hours in a silica crucible. Glass crusts were separated from lava blocks where possible, washed several times with deionized water, and mounted for major element analysis using a JEOL JXA 8900R electron microprobe (Universität Kiel) operating with a 10 μm defocused beam, beam current of 10 nA, acceleration voltage of 15 kV, and calibrated against natural glass standards. Precision and accuracy relative to VG-2 were both better than 1% (2σ) for all major elements. Glass fragment subsets were also ground in an agate mortar for trace element and isotopic determinations.

[10] For trace element determinations, 44 agate-ground powders were repeatedly digested in HF/HNO_3 and finally taken up in 2N HNO_3 for analysis in an upgraded VG PlasmaQuad ICP-MS (Universität Kiel) following the procedure outlined by *Garbe-Schönberg* [1993] (Table 1). Precision (2σ) for most trace elements was better than 3%, exceptions being the transition metals (Cr, Ni, Cu, Zn, Ga) and those elements at very low concentrations (e.g., Cs up to 20%). Accuracy was better than 10% for all elements relative to suggested values for BHVO-1 and BIR [*Jenner et al.*, 1990; *Govindaraju*, 1994] and generally better than 5% for the rare earth elements (REE).

[11] The Sr, Nd and Pb isotopic compositions of 22 samples were measured using a Finnigan MAT 262 RPQ2+ thermal ionization mass spectrometer at IFM–GEOMAR operating in static mode for Sr-Pb and multidynamic mode for Nd (Table 2). Powders were leached for 1 hour in hot 6 N HCl prior to dissolution in HF/HNO_3, and the analytical procedures followed those described by *Hoernle and Tilton* [1991]. Applied isotope fractionation corrections were $^{86}Sr/^{88}Sr = 0.1194$ and $^{146}Nd/^{144}Nd = 0.7219$, with all errors reported as 2σ standard errors of the mean (in run). Analyses of NBS 987 during the course of this study yielded $^{87}Sr/^{86}Sr = 0.710215 \pm 9$ (n = 6). Our reported Sr analyses (Table 2) are normalized to $^{87}Sr/^{86}Sr = 0.71025$ for NBS 987. For the in-house Nd monitor SPEX we obtained $^{143}Nd/^{144}Nd = 0.511711 \pm 11$ (n = 7). Previous calibrations of SPEX yielded $^{143}Nd/^{144}Nd = 0.511706 \pm 12$ (n = 10) against La Jolla at $^{143}Nd/^{144}Nd = 0.511848 \pm 8$ (n = 10). For Pb, all analyses were fractionation-corrected using repeated measurements of NBS 981 completed under the same loading and run conditions (n = 15; $^{206}Pb/^{204}Pb = 16.896 \pm 14$, $^{207}Pb/^{204}Pb = 15.435 \pm 15$, $^{208}Pb/^{204}Pb = 36.522 \pm 46$; mass fractionation ~0.12 per amu) and normalized to the values reported by *Todt et al.* [1996]. Total chemistry Pb blanks were negligible (<0.3 ng).

4. Geochemistry

[12] The new major and trace element analyses presented in Table 1 range from basalt to rhyolite and from subalkaline to alkaline. A wide compositional spectrum has previously been reported for central Bransfield Basin lavas [*Weaver et al.*, 1979; *Keller et al.*, 1991, 2002]. Our analyses demonstrate that a broad range of compositions also characterizes the eastern subbasin. Three distinct geochemical groups can be recognized (Figure 2):

[13] 1. Bransfield Group lavas are subalkaline, range in composition from basalt to rhyolite, and form a continuum from low-K series basalt to compositions straddling both the low-K and medium-K series at higher SiO_2. These lavas constitute the bulk of the recovered samples and were found at all stations except those on Gibbs Rise. Several subgroups are evident. Bridgeman Rise lavas form an array with steeper slope than the low-K to medium-K series boundary and the central Bransfield lava array of *Keller et al.* [2002]. In contrast, lavas from Spanish Rise are low-K basalt, those from Hook Ridge are low-K rhyodacite, and both of these overlap the central Bransfield array.

[14] 2. Gibbs Group lavas are subalkaline and range in composition from basaltic andesite to andesite. At 53–55 wt % SiO_2 they have ~2 wt % K_2O, compared to <0.8 wt % K_2O for Bransfield Group lavas. Gibbs Group lavas can be classified as members of the high-K series, and although their SiO_2 contents are lower, they have comparable K_2O concentrations to those of the South Shetland arc lavas. An exception is one chloritized andesite whose lower K_2O (appropriate for the medium-K series) probably reflects K mobilization during alteration (21DR-01). All Gibbs Group lavas were recovered from Gibbs Rise. They were more weathered than other Bransfield lavas and have higher LOI values (>1.5 wt %).

[15] 3. Alkali Group lavas are members of the alkaline series, range in composition from basalt to tephrite and have 2.1–10.8 wt % normative nepheline (calculated assuming $Fe_2O_3/FeO = 0.1$). The seven lavas in this group were recovered from five stations between Bridgeman Rise and Gibbs Rise. The Alkali Group lavas were single distinctive boulders in the dredge haul at four of these stations, and in

[1]Auxiliary material is available at ftp://ftp.agu.org/apend/jb/2004JB003046.

Table 1. Representative Major and Trace Element Analyses of Bransfield Basin Lavas[a]

	Hook Ridge Sample		Bridgeman Rise Samples												
	7GTV-01	38DR-01	2DR-01	3DR-01	3DR-02	3DR-05	3DR-07	3DR-08	3DR-09gl	3DR-11	3DR-14	4DR-01	4DR-07	4DR-09	4DR-13
Lat. (°S)	62°11.5′	62°10.9′	62°07.2′	62°07.0′	62°07.0′	62°07.0′	62°07.0′	62°07.0′	62°07.0′	62°07.0′	62°07.0′	62°03.6′	62°03.6′	62°03.6′	62°03.6′
Long. (°W)	57°16.6′	57°14.4′	57°00.6′	56°53.3′	56°53.3′	56°53.3′	56°53.3′	56°53.3′	56°53.3′	56°53.3′	56°53.3′	56°57.8′	56°57.8′	56°57.8′	56°57.8′
Depth (m)	1050	1335	1289	545	545	545	545	545	545	545	545	703	703	703	703
Group	Brans.	Brans.	Brans.	Brans.	Brans.	Brans.	Brans.	Brans.	Brans.	Brans.	Brans.	Brans.	Brans.	Brans.	Alkali
SiO_2	68.38	67.00	51.19	50.29	51.55	58.04	65.70	67.63	72.39	56.71	58.41	53.42	53.26	57.71	46.26
TiO_2	0.49	0.73	0.71	0.61	0.86	0.72	0.77	0.60	0.70	0.86	0.58	0.80	0.76	1.31	2.30
Al_2O_3	13.96	14.49	17.74	15.10	18.10	16.12	15.83	14.71	12.41	16.94	17.95	18.88	18.41	16.02	16.22
Fe_2O_3	5.82	5.10	7.57	7.73	7.88	6.19	4.44	3.85	4.60	7.79	4.89	7.84	7.86	9.81	10.32
MnO	0.16	0.15	0.12	0.13	0.13	0.11	0.07	0.07	0.09	0.14	0.06	0.12	0.13	0.16	0.14
MgO	0.48	0.91	6.65	11.70	6.72	4.10	0.98	0.71	0.57	4.14	4.01	4.76	5.54	2.37	7.28
CaO	2.55	2.88	12.13	10.34	11.56	6.55	3.34	2.55	1.65	8.34	7.27	10.13	10.27	6.15	7.97
Na_2O	6.11	5.52	2.47	2.23	2.94	5.06	5.28	5.22	3.90	3.73	3.84	3.22	3.06	4.33	4.61
K_2O	1.02	1.17	0.44	0.27	0.31	1.21	1.97	2.43	2.94	0.96	0.87	0.47	0.43	0.89	2.00
P_2O_5	0.12	0.18	0.08	0.05	0.09	0.13	0.15	0.11	0.17	0.13	0.13	0.08	0.07	0.16	0.93
LOI	0.72	0.98	0.23	−0.01	−0.41	−0.41	0.34	0.49		−0.11	1.28	−0.08	0.26	0.38	2.33
Total	99.78	99.11	99.33	98.44	99.73	97.82	98.87	98.37	99.42	99.63	99.29	99.64	100.05	99.29	100.36
Sc	17.6	9.17	31.8	29.7	30.7	31.4	10.0	8.49	14.6	24.9	16.6	25.4	28.0	24.1	18.1
Cr	0.91		59.9	378	156	158	1.29	0.11	0.83	85.9	56.1	42.6	52.4	0.40	171
Co	1.44	0.858	27.1	39.1	30.7	31.0	8.03	5.57	7.47	24.1	17.8	27.1	28.1	22.0	35.8
Ni	0.405		52.3	250	67.5	69.9	1.68	0.891	1.36	34.3	38.4	31.6	34.8	2.61	106
Cu	8.67	2.17	61.7	52.4	72.8	75.3	20.6	34.2	28.5	75.4	51.7	76.6	93.3	59.1	37.3
Zn	113	88.1	51.7	50.2	55.0	55.3	46.4	53.5	56.3	76.6	44.9	57.9	55.6	84.1	74.3
Rb	20.1	21.5	8.68	5.83	7.63	8.16	56.1	81.2	76.2	27.0	9.13	10.1	9.18	19.6	16.0
Sr	125	181	273	200	256	262	186	143	61.9	276	705	336	322	290	1112
Y	65.5	63.2	14.8	13.8	17.4	17.7	29.0	33.1	46.7	20.1	10.0	16.1	14.9	28.3	21.8
Zr	362	308	50.2	48.0	58.5	60.1	72.9	163	321	88.2	80.8	59.7	53.2	117	246
Nb	4.84	4.98	1.48	0.687	0.811	0.839	3.06	3.55	4.22	1.48	1.28	0.868	0.843	1.85	57.7
Cs	0.981	1.05	0.463	0.341	0.510	0.455	2.62	4.67	2.57	1.37	0.410	0.577	0.542	1.10	0.314
Ba	154	233	90.1	54.4	54.2	57.7	287	331	321	166	135	66.4	61.6	127	304
La	15.6	20.1	4.17	2.62	3.13	3.23	13.2	14.0	17.5	7.44	8.32	3.11	2.87	6.43	44.1
Ce	41.9	53.2	10.3	7.17	8.42	8.78	31.2	33.7	43.1	17.8	19.1	8.43	7.87	17.1	81.8
Pr	6.30	7.36	1.41	1.09	1.37	1.40	4.24	4.58	5.99	2.51	2.58	1.33	1.23	2.66	9.18
Nd	29.3	33.2	6.57	5.45	6.87	7.23	18.3	19.9	26.2	11.3	10.9	6.82	6.35	13.4	34.6
Sm	8.43	8.77	1.92	1.74	2.30	2.30	4.69	5.14	7.02	3.13	2.44	2.23	2.05	4.12	6.89
Eu	2.04	2.14	0.674	0.632	0.853	0.903	1.18	1.07	0.932	0.952	0.781	0.856	0.803	1.36	2.19
Gd	9.72	9.36	2.25	2.10	2.82	2.92	4.91	5.55	7.57	3.47	2.27	2.72	2.57	4.96	6.04
Tb	1.73	1.66	0.395	0.369	0.502	0.513	0.827	0.935	1.29	0.585	0.339	0.483	0.450	0.845	0.861
Dy	11.4	10.8	2.58	2.41	3.29	3.42	5.41	6.08	8.49	3.81	1.99	3.16	2.92	5.56	4.76
Ho	2.39	2.29	0.541	0.508	0.701	0.718	1.12	1.26	1.78	0.806	0.404	0.649	0.611	1.13	0.875
Er	7.00	6.76	1.54	1.45	1.96	2.01	3.15	3.65	5.16	2.23	1.10	1.83	1.71	3.22	2.24
Tm	1.06	1.01	0.222	0.211	0.295	0.294	0.466	0.540	0.784	0.333	0.156	0.267	0.251	0.474	0.302
Yb	7.13	6.86	1.48	1.42	1.92	1.94	3.10	3.66	5.27	2.24	1.04	1.75	1.63	3.10	1.89
Lu	1.07	1.02	0.222	0.208	0.290	0.287	0.447	0.529	0.797	0.338	0.151	0.259	0.242	0.463	0.269
Hf	9.24	9.22	1.67	1.55	1.84	1.85	3.13	5.10	9.35	2.88	2.30	1.83	1.66	3.53	5.04
Ta	0.336	0.387	0.100	0.051	0.057	0.061	0.223	0.264	0.306	0.103	0.085	0.064	0.103	0.134	3.05
Tl	0.172	0.190	0.070	0.042	0.038	0.041	0.209	0.432	0.274	0.172	0.032	0.061	0.054	0.125	0.036

Table 1. (continued)

	Hook Ridge Sample		Bridgeman Rise Samples													
	7GTV-01	38DR-01	2DR-01	3DR-01	3DR-02	3DR-05	3DR-07	3DR-08	3DR-09gl	3DR-11	3DR-14	4DR-01	4DR-07	4DR-09	4DR-13	
Pb	6.50	7.01	3.31	1.92	1.90	1.88	6.38	11.3	7.64	6.03	2.94	2.62	2.41	4.87	3.33	
Th	3.46	4.54	0.971	0.561	0.663	0.677	5.58	7.01	7.76	2.49	2.20	0.681	0.608	1.48	4.74	
U	1.08	1.23	0.318	0.218	0.223	0.232	1.48	1.86	2.432	0.719	0.579	0.283	0.269	0.592	1.74	
	G Ridge Sample											Spanish Rise Samples				
	13DR-02	13DR-03	14DR-01	14DR-06	15DR-01gl	16DR-01	16DR-02	16DR-11	17DR-01	17DR-02	17DR-06	18DR-01	18DR-09	25DR-02	25DR-04	25DR-06	26DR-01
Lat. (°S)	62°06.7′	62°06.7′	62°04.2′	62°04.2′	62°02.4′	62°00.1′	62°00.1′	62°00.1′	61°58.4′	61°58.4′	61°58.4′	61°52.8′	61°52.8′	61°53.4′	61°53.4′	61°53.4′	61°55.6′
Long. (°W)	56°30.9′	56°30.9′	56°23.3′	56°23.3′	56°19.6′	56°14.1′	56°14.1′	56°14.1′	56°10.8′	56°10.8′	56°10.8′	55°59.0′	55°59.0′	55°48.9′	55°48.9′	55°48.9′	55°53.3′
Depth (m)	1039	1039	1177	1177	1834	2125	2125	2125	2332	2332	2332	1421	1421	2130	2130	2130	1771
Group	Brans.	Brans.	Brans.	Alkali	Brans.	Brans.	Brans.	Brans.	Brans.	Brans.	Brans.	Brans.	Brans.	Brans.	Brans.P.	Alkali	Alkali
SiO_2	65.12	51.26	47.88	47.22	50.84	50.27	50.54	63.28	50.09	53.46	53.92	51.14	51.37	49.61	49.12	47.79	45.89
TiO_2	0.85	1.18	1.21	1.94	1.77	1.19	1.19	1.05	1.31	1.41	1.62	0.60	0.60	1.32	1.88	2.01	2.15
Al_2O_3	11.54	16.85	17.29	15.00	14.96	16.65	16.79	15.30	16.61	15.31	16.14	15.44	15.62	15.91	15.86	15.11	15.36
Fe_2O_3	6.32	9.49	9.44	12.22	11.10	8.70	8.75	6.79	9.11	9.76	10.51	7.86	7.70	8.83	10.17	11.60	11.82
MnO	0.10	0.15	0.14	0.17	0.18	0.12	0.13	0.14	0.14	0.19	0.16	0.13	0.13	0.14	0.16	0.16	0.16
MgO	3.67	5.80	7.78	9.10	5.50	6.49	7.11	1.47	6.66	5.17	3.66	10.71	10.49	9.85	7.71	8.79	8.92
CaO	7.02	10.58	12.36	8.74	10.15	11.58	11.55	4.02	11.22	8.77	7.79	9.46	9.55	9.32	9.99	8.53	8.02
Na_2O	2.14	3.25	2.85	3.74	3.21	2.57	2.72	5.21	2.83	3.94	4.42	2.78	2.84	3.47	3.75	3.45	4.14
K_2O	0.26	0.38	0.44	1.21	0.38	0.39	0.48	1.53	0.51	0.56	0.34	0.41	0.41	0.47	0.38	1.21	1.52
P_2O_5	0.09	0.09	0.11	0.44	0.24	0.13	0.15	0.24	0.15	0.20	0.15	0.08	0.08	0.20	0.25	0.45	0.66
LOI	1.62	−0.08	−0.02	−0.60		0.27	0.46	−0.10	0.46	0.46	0.22	0.02	0.32	0.13	0.12	−0.23	1.25
Total	98.72	98.95	99.48	99.18	98.34	98.36	99.87	98.93	99.09	99.23	98.93	98.63	99.11	99.25	99.39	98.87	99.86
Sc	21.3	33.4	32.7	21.1	33.1	30.4	30.6	15.9	32.8	26.5	25.5	29.4	28.1	38.1	31.9	23.3	19.4
Cr	25.8	23.5	17.8	278	109	170	167	1.38	162	134	30.3	386	334	446	221	298	228
Co	18.5	32.6	33.1	48.9	33.9	28.7	32.6	9.44	34.6	26.1	27.3	41.0	37.6	43.7	33.7	45.9	46.0
Ni	11.4	22.6	21.4	171	50.2	44.0	57.3	1.02	56.6	44.3	10.5	250	242	242	104	156	179
Cu	31.9	52.6	52.0	42.9	60.2	53.4	56.1	45.1	62.2	38.6	20.5	59.9	53.0	48.1	53.1	41.8	46.6
Zn	44.0	62.4	63.1	92.9	63.3	54.7	54.9	81.6	59.9	86.4	72.4	57.4	54.5	68.7	71.4	89.8	84.5
Rb	4.59	8.70	8.46	15.2	7.86	7.26	10.6	45.9	10.1	7.83	4.31	9.05	9.32	6.19	2.48	18.4	14.4
Sr	239	274	275	539	304	366	399	198	332	163	255	210	212	248	252	597	758
Y	15.1	19.6	19.8	21.5	18.8	19.0	18.7	37.1	21.7	39.8	33.0	13.0	13.3	25.9	35.6	23.9	22.2
Zr	56.1	76.0	76.5	174	72.8	83.3	91.5	188	96.0	156	148	54.2	55.6	142	176	179	230
Nb	1.33	1.22	1.22	31.4	1.63	1.34	1.37	2.63	1.46	2.92	2.16	0.933	0.942	3.38	4.13	29.2	36.6
Cs	0.614	0.474	0.512	0.280	0.360	0.223	0.275	3.02	0.279	0.306	0.175	0.436	0.386	0.140	0.071	0.609	0.258
Ba	573	55.3	54.8	152	54.3	128	131	243	112	49.8	90.3	80.2	83.6	34.2	27.4	168	161
La	3.39	3.76	3.75	22.2	4.44	10.6	11.1	12.0	9.49	6.51	7.21	3.55	3.68	6.19	7.65	22.1	28.7
Ce	9.33	10.4	10.4	45.2	12.0	26.7	26.8	29.6	23.5	19.7	19.8	8.60	9.07	17.3	23.2	46.6	58.4
Pr	1.38	1.67	1.67	5.45	1.81	3.56	3.70	4.24	3.33	3.24	3.11	1.29	1.32	2.66	3.50	5.63	6.94
Nd	6.82	8.34	8.41	22.2	8.99	15.6	16.2	19.7	15.2	16.8	15.2	6.15	6.45	12.6	17.0	23.2	27.9
Sm	2.08	2.68	2.70	5.00	2.72	3.71	3.78	5.49	3.89	5.32	4.54	1.83	1.91	3.63	4.92	5.38	5.88
Eu	0.797	1.03	1.02	1.68	1.09	1.17	1.23	1.45	1.29	1.96	1.62	0.666	0.679	1.25	1.66	1.78	1.95
Gd	2.48	3.29	3.28	5.06	3.29	3.55	3.87	6.08	4.17	6.51	5.35	2.17	2.30	4.23	5.60	5.34	5.70
Tb	0.421	0.578	0.577	0.786	0.574	0.571	0.609	1.04	0.685	1.18	0.943	0.377	0.385	0.731	0.984	0.814	0.850
Dy	2.71	3.83	3.90	4.66	3.72	3.51	3.87	6.85	4.33	7.80	6.28	2.51	2.61	4.65	6.33	4.75	4.86
Ho	0.564	0.796	0.817	0.882	0.762	0.709	0.765	1.44	0.879	1.65	1.31	0.528	0.542	0.971	1.32	0.900	0.916
Er	1.57	2.25	2.28	2.34	2.15	1.96	2.10	4.13	2.44	4.58	3.71	1.51	1.54	2.72	3.72	2.39	2.36
Tm	0.226	0.325	0.337	0.317	0.306	0.275	0.303	0.626	0.357	0.671	0.548	0.223	0.230	0.404	0.538	0.324	0.328
Yb	1.48	2.16	2.23	1.99	2.01	1.80	1.95	4.20	2.29	4.44	3.71	1.52	1.51	2.63	3.54	2.04	2.04

Table 1. (continued)

	G Ridge Sample							Spanish Rise Samples									
	13DR-02	13DR-03	14DR-01	14DR-06	15DR-01gl	16DR-01	16DR-02	16DR-11	17DR-01	17DR-02	17DR-06	18DR-01	18DR-09	25DR-02	25DR-04	25DR-06	26DR-01
Lu	0.220	0.319	0.330	0.296	0.299	0.262	0.288	0.636	0.340	0.670	0.548	0.226	0.235	0.390	0.516	0.287	0.302
Hf	1.62	2.16	2.21	3.94	2.00	2.50	2.61	5.60	2.64	4.20	3.83	1.69	1.74	3.28	4.38	3.71	4.87
Ta	0.100	0.098	0.092	1.97	0.116	0.103	0.100	0.181	0.111	0.219	0.152	0.061	0.063	0.231	0.313	1.56	2.26
Tl	2.62	0.058	0.057	0.038	0.071	0.077	0.093	0.191	0.118	0.098	0.029	0.046	0.052	0.102	0.032	0.061	0.044
Pb	1.81	2.00	2.02	2.11	1.89	1.97	1.83	7.83	1.74	1.85	1.88	1.65	1.72	1.12	1.15	2.90	2.30
Th	0.514	0.724	0.746	2.74	0.679	2.67	2.75	3.97	2.22	0.613	1.10	0.821	0.924	0.447	0.468	2.71	2.83
U	0.608	0.247	0.247	0.991	0.218	0.536	0.529	1.29	0.416	0.274	0.388	0.257	0.279	0.187	0.443	0.927	1.17

	Spanish Rise Sample						Gibbs Rise Sample						Standards			
													VG-2, $n = 20$ BIR, $n = 3$		BHVO-1, $n = 10$ BHVO-1, $n = 4$	
	26DR-03	26DR-05	27DR-01	27DR-04	28DR-01	28DR-10	20DR-01	20DR-02	21DR-01	23DR-02	23DR-10	23DR-12	Average	σ	Average	σ
Lat. (°S)	61°55.6′	61°55.6′	61°57.6′	61°57.6′	61°59.3′	61°59.3′	61°48.6′	61°48.6′	61°49.9′	61°45.7′	61°45.7′	61°45.7′				
Long. (°W)	55°53.3′	55°53.3′	55°52.2′	55°52.2′	55°53.8′	55°53.8′	55°28.6′	55°28.6′	55°28.4′	55°25.0′	55°25.0′	55°25.0				
Depth (m)	1771	1771	1800	1800	1850	1850	2505	2505	1480	2400	2400	2400				
Group	Alkali	Alkali	Brans.P.	Brans.	Brans.P.	Brans.	Alkali	Gibbs	Gibbs	Gibbs	Gibbs	Gibbs				
SiO_2	47.47	46.00	50.35	50.74	50.02	48.20	44.39	55.78	57.54	54.15	53.55	53.46	50.41	0.20	49.91	0.22
TiO_2	1.75	2.03	1.49	1.48	1.20	1.17	2.57	0.78	0.78	0.82	0.80	0.78	1.86	0.08	2.75	0.02
Al_2O_3	15.42	15.09	17.28	17.01	16.16	16.99	14.87	16.74	17.87	18.71	18.45	18.95	13.82	0.09	13.58	0.08
Fe_2O_3	10.67	12.38	8.45	8.55	8.46	10.20	12.12	6.65	6.36	7.75	7.53	7.04	12.92	0.22	12.21	0.14
MnO	0.15	0.17	0.14	0.14	0.15	0.16	0.14	0.12	0.10	0.09	0.10	0.11	0.20	0.04	0.16	0.00
MgO	8.35	8.54	6.37	6.13	9.67	7.08	8.63	4.30	4.51	2.74	2.54	2.05	6.65	0.07	7.20	0.04
CaO	8.07	9.42	10.90	10.49	10.19	8.88	8.02	5.13	7.07	8.25	8.06	8.39	10.85	0.11	11.42	0.06
Na_2O	3.29	3.08	3.69	3.56	3.15	3.43	3.58	3.74	3.61	3.12	3.46	3.02	2.59	0.04	2.49	0.14
K_2O	1.45	0.99	0.39	0.39	0.40	0.33	2.09	2.79	0.88	2.21	1.88	2.04	0.19	0.02	0.53	0.02
P_2O_5	0.40	0.43	0.18	0.19	0.17	0.33	0.69	0.15	0.14	0.26	0.28	0.24	0.30	0.02	0.28	0.01
LOI	1.09	0.88	−0.23	−0.10	0.19	3.24	1.74	3.28	2.17	1.67	2.74	1.98				
Total	98.12	99.01	99.01	98.57	99.74	100.01	98.84	99.46	101.03	99.77	99.39	98.07				
Sc	22.5	31.7	32.8	31.5	29.9	27.1	21.2	19.9	23.53	18.8	19.7	18.0	42.44	1.02	29.9	1.81
Cr	290	364	153	143	274	245	205	53.4	48.14	4.73	8.01	4.71	384	18.60	280	19.60
Co	37.6	51.3	30.9	30.0	38.4	36.1	47.8	16.2	17.6	14.1	17.2	11.1	51.9	1.06	43.5	1.01
Ni	135	137	50.3	47.7	168	119	171	23.7	17.2	1.90	6.33		168	2.01	119	7.36
Cu	39.6	52.9	50.7	53.6	57.3	61.9	44.2	67.7	136	128	147	132	116	2.45	131	4.81
Zn	81.7	97.0	63.9	63.7	58.1	79.6	90.1	73.7	57.8	60.4	67.2	58.9	66.5	1.72	102	5.85
Rb	14.5	9.62	4.14	6.53	5.72	2.21	16.9	43.9	12.2	32.1	43.9	54.0	0.24	0.02	10.8	0.20
Sr	485	536	290	282	258	433	917	301	370	409	680	444	111	2.12	397	2.72
Y	21.6	22.2	25.2	24.8	20.8	21.0	22.0	17.5	20.2	18.7	19.5	17.7	14.7	0.13	24.2	0.32
Zr	164	145	133	132	108	95.8	247	75.7	105	127	146	123	14.4	0.16	168	2.09
Nb	23.2	24.4	3.08	3.32	2.92	5.15	41.8	2.32	2.78	2.89	3.16	2.78	0.504	0.016	16.9	0.10
Cs	0.145	0.263	0.137	0.343	0.244	0.039	0.323	0.437	0.869	1.54	3.82	3.51	0.006	0.002	0.119	0.019
Ba	199	105	30.2	45.9	43.9	174	185	441	285	497	496	475	6.72	0.15	133	1.57
La	17.9	18.5	5.56	6.14	5.48	11.1	32.1	11.3	12.0	19.0	20.7	18.3	0.627	0.008	15.3	0.22
Ce	39.4	39.1	16.0	17.3	14.6	25.9	66.2	25.8	28.2	42.8	44.6	40.9	1.95	0.02	38.1	0.53
Pr	4.77	4.90	2.53	2.65	2.20	3.64	8.01	3.35	3.69	5.19	5.58	4.95	0.385	0.004	5.46	0.08
Nd	20.0	20.6	12.3	12.6	10.4	16.4	31.6	14.4	15.9	21.2	23.0	20.2	2.44	0.03	24.9	0.36
Sm	4.65	4.93	3.66	3.70	3.10	4.25	6.80	3.50	3.83	4.52	4.88	4.33	1.15	0.01	6.27	0.11
Eu	1.55	1.67	1.33	1.31	1.12	1.36	2.21	0.975	1.10	1.12	1.22	1.08	0.537	0.008	2.11	0.04

Table 1. (continued)

	Spanish Rise Sample						Gibbs Rise Sample						Standards			
													VG-2, n = 20 BIR, n = 3		BHVO-1, n = 10 BHVO-1, n = 4	
	26DR-03	26DR-05	27DR-01	27DR-04	28DR-01	28DR-10	20DR-01	20DR-02	21DR-01	23DR-02	23DR-10	23DR-12	Average	σ	Average	σ
Gd	4.46	5.13	4.32	4.30	3.66	4.17	6.11	3.36	3.70	3.87	4.35	3.67	1.88	0.02	6.30	0.12
Tb	0.704	0.787	0.748	0.748	0.624	0.664	0.888	0.528	0.596	0.574	0.626	0.545	0.372	0.004	0.957	0.020
Dy	4.19	4.58	4.99	4.90	4.10	4.09	4.89	3.17	3.62	3.37	3.82	3.21	2.72	0.02	5.53	0.11
Ho	0.820	0.861	1.04	1.03	0.843	0.829	0.902	0.635	0.735	0.680	0.776	0.644	0.596	0.005	1.02	0.01
Er	2.20	2.26	2.92	2.91	2.34	2.29	2.31	1.82	2.08	1.92	2.20	1.83	1.74	0.02	2.56	0.06
Tm	0.306	0.312	0.427	0.422	0.339	0.333	0.313	0.252	0.300	0.280	0.325	0.265	0.258	0.001	0.338	0.008
Yb	2.00	1.94	2.83	2.82	2.24	2.23	1.95	1.66	2.03	1.89	2.13	1.78	1.73	0.02	2.05	0.03
Lu	0.289	0.279	0.420	0.406	0.335	0.337	0.280	0.241	0.300	0.278	0.325	0.264	0.257	0.005	0.286	0.005
Hf	4.00	3.41	3.27	3.25	2.62	2.37	5.30	2.65	3.36	3.97	4.26	3.84	0.606	0.006	4.51	0.08
Ta	1.46	1.41	0.229	0.247	0.199	0.30	2.55	0.17	0.20	0.19	0.21	0.19	0.037	0.001	1.11	0.02
Tl	0.007	0.039	0.066	0.038	0.090	0.007	0.025	0.398	0.116	0.141	0.161	0.239	0.001	0.001	0.043	0.003
Pb	2.54	1.59	1.01	1.79	1.22	3.55	2.39	4.22	4.64	15.4	14.6	14.1	3.13	0.03	2.12	0.08
Th	2.17	1.83	0.328	0.655	0.874	0.661	2.67	3.25	3.66	9.33	10.1	9.00	0.029	0.002	1.28	0.06
U	0.751	0.666	0.215	0.254	0.378	0.175	1.06	0.872	1.07	2.26	2.77	2.36	0.010	0.001	0.443	0.012

[a]Sample co-ordinates are dredge mid-points (~500 m ground tracks). Major elements analyzed by XRF and reported in wt % with total Fe as Fe_2O_3, except for those with suffix gl and VG-2 (glasses analyzed by electron microprobe); averaged data are presented for samples 3DR-09gl (8 analyses), 15DR-01gl (15 analyses), and 7GTV-01, 25DR-04, 26DR-01, 27DR-04, 28DR-01 (2 analyses). Trace elements analyzed by ICP-MS and reported in ppm. See text for definition of the geochemical groups (Brans. = Bransfield; Brans.P. = Bransfield Primitive subgroup).

two instances they were red and oxidized. This suggests they were erupted in a subaerial environment and later transported to their respective stations on Bridgeman Rise and Gibbs Rise, where present-day water depths exceed 700 m. At the remaining station (26DR, Spanish Rise), Alkali Group lavas were the only fresh samples in a large haul bearing an exceptionally high proportion of glacial erratics (95% mica schists, chloritized lavas and sediments similar to those outcropping on the nearby Elephant and Gibbs Islands). We caution that the in situ status of all Alkali Group lavas is unproven, although their fresh condition (including pristine olivine phenocrysts), abundance and distribution attest to a recent source on or near Spanish Rise.

[16] Major element covariations with MgO highlight differences both among Bransfield Group lavas from different volcanic centers and between the three groups (Figure 3). Bridgeman Rise lavas have $Ti_{7.0}$ = 0.8 wt % (where $Ti_{7.0} = TiO_2$ at 7 wt % MgO), G Ridge lavas have $Ti_{7.0}$ = 1.3 wt %, and Spanish Rise lavas have $Ti_{7.0}$ = 1.6 wt %. Furthermore, Bridgeman Rise lavas have nearly constant TiO_2 as MgO decreases from 12 to 1 wt %, whereas for Spanish Rise lavas TiO_2 increases from 0.6 to 2.0 wt % as MgO decreases from 11 to 6 wt %. These changes are inversely reflected in FeO*/TiO_2 (where FeO* = all Fe as FeO), as Bridgeman Rise lavas have Fe*/$Ti_{7.0} \sim 9$, G Ridge lavas have Fe*/$Ti_{7.0} \sim 6.5$, and Spanish Rise lavas have Fe*/$Ti_{7.0} \sim 5$ (although a subset with >10% MgO plot along an extension of the Bridgeman Rise trend). Gibbs Group lavas overlap the array for Bridgeman Rise lavas in TiO_2-MgO space, whereas Alkali Group lavas have the highest TiO_2 contents and cover the range from 1.8–2.7 wt % TiO_2 at ~9 wt % MgO. Similar variations in $Ti_{7.0}$ and Fe*/$Ti_{7.0}$ occur between the individual volcanic centers of the central Bransfield Basin [*Keller et al.*, 2002]. We infer that each volcanic center is characterized by either a different mantle source composition or degree of partial melting, and that subsequent fractional crystallization takes place under different oxygen fugacities at each center.

[17] Volcanic centers in the NE part of the central Bransfield Basin (east of 58°20′W) have lower Na_2O ($Na_{7.0}$ < 3 wt %) and lower Na_2O/K_2O ($Na/K_{7.0}$ < 12) than those farther SW [*Keller et al.*, 2002]. The new Bransfield Group analyses from Bridgeman Rise and G Ridge have $Na_{7.0}$ = 2.8 wt % and $Na/K_{7.0}$ < 10, consistent with their location in the eastern Bransfield Basin. However, lavas from Spanish Rise have $Na_{7.0}$ = 3.8 wt % and are even more sodic than lavas from the SW central Bransfield Basin (Figure 3c). Nevertheless, Spanish Rise lavas share the low eastern Bransfield value of $Na/K_{7.0}$ = 10, and they also display an unusual trend of increasing Na_2O/K_2O with decreasing MgO (Figure 3d). Both Gibbs Group and Alkali Group lavas have significantly lower Na_2O/K_2O than Bransfield Group lavas (<4).

[18] Trace element concentrations in Bransfield Group lavas, in particular the LILE, show considerable scatter at any MgO content and for individual volcanic centers. Less scatter is shown by the HFSE, and HFSE concentrations at 7 wt % MgO consistently increase to the NE from Bridgeman Rise to G Ridge, and more markedly to Spanish Rise. For example, $Nb_{7.0}$ = 1 for Bridgeman Rise, 1.5 for G Ridge and 4 for Spanish Rise. *Keller et al.* [2002] have previously noted that HFSE concentra-

Table 2. Sr-Nd-Pb Isotopic Composition of Bransfield Basin Lavas[a]

Sample	$^{87}Sr/^{86}Sr$	2σ	$^{143}Nd/^{144}Nd$	2σ	$^{206}Pb/^{204}Pb$	2σ	$^{207}Pb/^{204}Pb$	2σ	$^{208}Pb/^{204}Pb$	2σ
					Hook Ridge					
07GTV-01	0.703069	6	0.513019	8	18.734	1	15.578	1	38.396	1
38DR-01	0.703198	8	0.512982	9	18.750	1	15.586	1	38.437	1
					Bridgeman Rise					
02DR-01	0.703568	6	0.512948	12	18.744	1	15.583	1	38.448	1
03DR-01	0.703322	8	nd		18.750	7	15.593	6	38.483	2
03DR-09gl	0.703354	8	0.512930	8	18.744	1	15.592	1	38.471	1
04DR-01	0.703189	6	nd		18.731	1	15.579	1	38.422	2
04DR-09	0.703219	6	0.512965	8	18.726	1	15.571	1	38.395	2
					G Ridge					
13DR-03	0.703156	9	0.512986	8	18.754	3	15.584	3	38.444	6
14DR-01	0.703290	10	nd		18.744	1	15.583	1	38.450	2
15DR-01	0.703131	8	0.512986	11	18.744	1	15.577	1	38.412	2
16DR-01	0.703146	6	nd		18.729	5	15.575	4	38.380	2
17DR-01	0.703154	6	0.512919	8	18.754	1	15.587	1	38.424	1
					Spanish Rise					
18DR-01	0.703507	7	0.512944	7	18.712	1	15.577	1	38.388	1
25DR-04gl	0.702662	9	0.513075	10	18.659	1	15.534	1	38.125	3
25DR-06	0.703439	2	0.512879	3	18.865	3	15.589	3	38.483	4
26DR-03	0.703493	9	0.512873	8	18.841	1	15.581	1	38.441	1
26DR-05	0.703146	2	0.512920	3	19.016	1	15.603	1	38.585	3
27DR-01	0.702593	8	0.513092	8	18.678	1	15.542	1	38.162	2
28DR-01	0.702731	8	0.513073	10	18.673	1	15.565	1	38.280	2
					Gibbs Rise					
20DR-02	0.704288	8	0.512922	7	18.727	1	15.578	1	38.429	1
21DR-01	0.703811	8	0.512914	7	18.711	1	15.569	1	38.392	1
23DR-02	0.703690	5	0.512845	8	18.694	1	15.603	1	38.496	1

[a]Isotope ratios for Sr normalized to NBS 987 ($^{87}Sr/^{86}Sr = 0.71025$) and for Pb to NBS 981 [*Todt et al.*, 1996]. Errors are 2σ standard errors of the mean and refer to in-run statistics; nd, not determined.

tions, like Na_2O, are highest in the SW central Bransfield Basin lavas and decrease to the NE. The new combined data set indicates that variations in both the HFSE and Na_2O along Bransfield Basin are broadly symmetric, with the highest concentrations in the SW central Bransfield Basin and at Spanish Rise separated by relatively low concentrations near Bridgeman Rise. Gibbs Group lavas have higher LILE concentrations at any given MgO than Bransfield Group lavas, but comparable HFSE levels. Alkali Group lavas are readily distinguished by their higher HFSE concentrations, in particular they have Nb > 20 ppm whereas Bransfield and Gibbs Group lavas have Nb < 5 ppm.

[19] Distinctly different chondrite-normalized REE patterns characterize each of the three geochemical groups (Figure 4). Bransfield Group lavas are weakly LREE-enriched with $(La/Yb)_N = 1.1–4.2$ (excluding one outlier from Bridgeman Rise with $(La/Yb)_N = 5.8$), and the full range is present at Bridgeman Rise, G Ridge and Spanish Rise. Negative Eu anomalies develop with increasing SiO_2, but significant anomalies (Eu/Eu* < 0.95) are restricted to lavas with >56 wt % SiO_2. Dacite from both Hook Ridge and Bridgeman Rise typically has Eu/Eu* = 0.60–0.75. In contrast, Gibbs Group lavas are moderately LREE-enriched with $(La/Yb)_N = 4.3–7.4$ and have negative Eu anomalies that are deeper than those of Bransfield Group lavas at comparable SiO_2 (Eu/Eu* = 0.8–0.9 compare Bransfield Group ~0.9). Alkali Group lavas are strongly LREE-enriched with $(La/Yb)_N = 6.4–16.8$ and lack any Eu anomaly. No Ce anomalies were evident for any analyzed lavas.

[20] All Bransfield and Gibbs Group lavas show strong enrichment in LILE relative to NMORB coupled with high values of LILE relative to HREE and HFSE (Figure 5). As Rb, Ba and other LILE are mobile in slab-derived fluids, whereas Yb, other HREE and HFSE are not, this enrichment is attributed to the transfer of a slab-derived fluid to the sub-Bransfield mantle [e.g., *Pearce and Peate*, 1995]. High levels of Th relative to HREE and HFSE may indicate a role for transfer of a sediment melt in addition to the slab-derived fluid, as experimental evidence suggests Th mobility requires a sediment melt rather than a slab-derived fluid [*Johnson and Plank*, 1999]. Bransfield Group lavas approximate the classic subduction-related pattern and have $(Rb/Yb)_{MORB}$, $(Ba/Yb)_{MORB}$ and $(Th/Yb)_{MORB}$ in the range 2–110. However, their HFSE concentrations range from slightly depleted to mildly enriched relative to HREE, with $(Nb/Yb)_{MORB} = 0.5–1.5$ (excluding one outlier at 2.6) and $(Zr/Yb)_{MORB} = 0.9–2.9$, and they do not exhibit a consistent negative Ta-Nb anomaly relative to the HREE. The new analyses mostly overlap the range previously reported for central Bransfield Basin lavas [*Keller et al.*, 2002], but extend to higher LILE/MORB and lower HFSE/MORB values (Figure 5a). We define the Bransfield Primitive subgroup as comprising the three Bransfield Group lavas with the least enrichment in LILE relative to the HREE (they have $(Rb/Yb)_{MORB}$, $(Ba/Yb)_{MORB}$ and $(Th/Yb)_{MORB}$ in the range 2–8 and $(Nb/Yb)_{MORB} = 1.2–1.5$), and contend

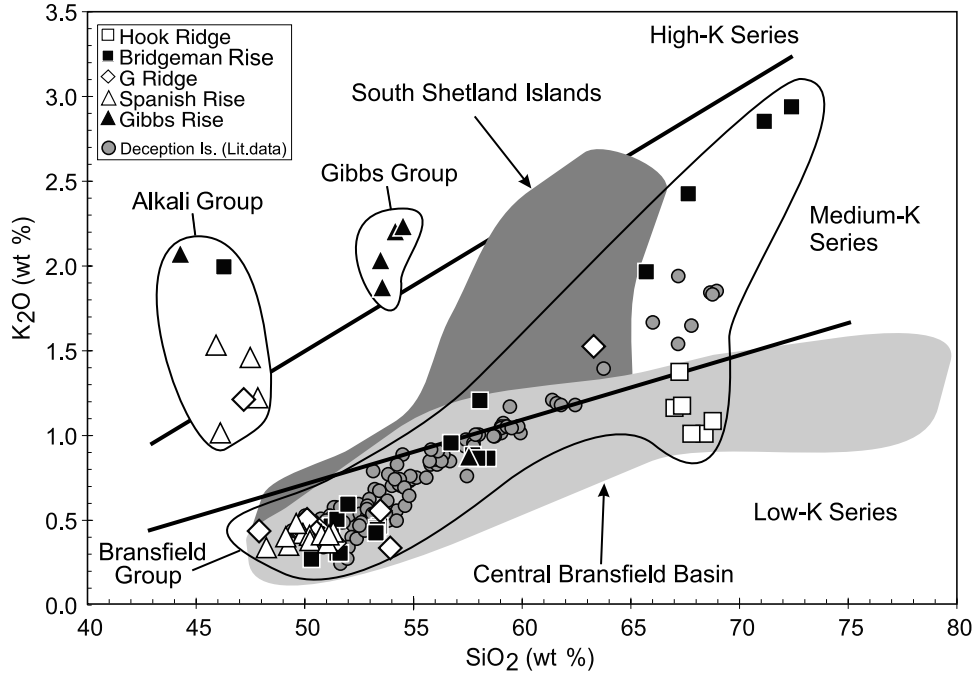

Figure 2. K_2O versus SiO_2 plot for lavas recovered during SO-155. Series boundaries are after *Peccerillo and Taylor* [1976]. Data for Deception Island are from *Baker et al.* [1975], *Weaver et al.* [1979], *Keller et al.* [1991], and *Smellie et al.* [1992]. Compositional fields for the central Bransfield Basin and South Shetland Islands are constructed from analyses of *Tarney et al.* [1982], *Saunders and Tarney* [1984], *Smellie et al.* [1984], *Fisk* [1990], and *Keller et al.* [1991, 2002].

that these lavas have the least subduction-related component (Figure 5b). This subgroup, which is spatially restricted to Spanish Rise, also has the least radiogenic Sr, Nd and Pb isotope values (see below). Gibbs Group lavas have similar NMORB normalized patterns to the main Bransfield Group lavas, with $(Rb/Yb)_{MORB}$, $(Ba/Yb)_{MORB}$ and $(Th/Yb)_{MORB}$ in the range 20–110, and their HFSE concentrations are mildly enriched relative to the HREE with $(Nb/Yb)_{MORB}$ = 1.5–1.7 and $(Zr/Yb)_{MORB}$ = 1.7–2.6. Their generally higher LILE/MORB values, especially for K and Pb, are comparable to those of South Shetland arc lavas (Figure 5a).

[21] In marked contrast to the Bransfield and Gibbs Group lavas, the Alkali Group lavas have a relatively smooth NMORB normalized pattern in which the degree of enrichment for any element relative to NMORB (or the HREE) is proportional to the incompatibility of the element during mantle melting (Figure 5c). For these lavas, $(Rb/Yb)_{MORB}$, $(Ba/Yb)_{MORB}$ and $(Th/Yb)_{MORB}$ are in the range 15–50, $(Nb/Yb)_{MORB}$ = 13–34, and $(Zr/Yb)_{MORB}$ = 2.8–4.9. Smooth NMORB normalized patterns have not been reported for any lavas previously recovered from the Bransfield Basin, but do characterize alkali basalts from James Ross Island, Seal Nunataks and Alexander Island [*Hole et al.*, 1993, 1995].

[22] Isotopic determinations for the eastern Bransfield Basin lavas cover a considerable range (Table 2 and Figures 6 and 7). Bransfield Group lavas form an array in Sr-Nd space extending from compositions that overlap the Pacific and South Atlantic MORB fields (for the Bransfield Primitive subgroup) to more radiogenic values ($^{87}Sr/^{86}Sr$ = 0.7026–0.7036, $^{143}Nd/^{144}Nd$ = 0.5131–0.5129). The Bransfield Primitive subgroup also have Pb isotope compositions that plot within the Pacific and South Atlantic MORB fields, whereas all other Bransfield Group lavas have higher $^{206}Pb/^{204}Pb$, $^{207}Pb/^{204}Pb$ and $^{208}Pb/^{204}Pb$ values and define an array with steeper slope than the Pacific and South Atlantic MORB fields for both $^{207}Pb/^{204}Pb$ and $^{208}Pb/^{204}Pb$ versus $^{206}Pb/^{204}Pb$ (Figures 6b and 6c). It has been proposed that mantle with Pacific isotope character is progressively replacing South Atlantic mantle and flowing eastward beneath the Drake Passage [*Pearce et al.*, 2001]. Pacific and South Atlantic MORB, and by inference their mantle sources, are most clearly discriminated on a plot of $^{143}Nd/^{144}Nd$ versus $^{206}Pb/^{204}Pb$ (Figure 7b). No Bransfield Basin lavas can be classified as MORB, but they can be modeled as melts of a mantle source contaminated by a subduction-related component of variable magnitude. Lavas of the Bransfield Primitive subgroup have the lowest LILE/HFSE values, least radiogenic isotopic compositions, and are the most MORB-like. These lavas have Pacific mantle isotope characteristics, and extrapolating a best fit mixing curve through the Bransfield Group array yields a mantle end-member that plots farther within the Pacific mantle field (Figure 7b). We infer that Pacific mantle has underlain the Bransfield Basin since its inception at ~3 Ma.

[23] Gibbs Group lavas have more radiogenic Sr and Nd isotopic compositions than Bransfield Group lavas ($^{87}Sr/^{86}Sr$ = 0.7037–0.7043, $^{143}Nd/^{144}Nd$ = 0.5129–0.5128), but comparable Pb isotope compositions (Figure 6). Alkali Group lavas are distinguished by their higher $^{206}Pb/^{204}Pb$ values but comparable $^{207}Pb/^{204}Pb$ and $^{208}Pb/^{204}Pb$ relative to all other Bransfield lavas ($^{206}Pb/^{204}Pb$ = 18.84–19.02 versus $^{206}Pb/^{204}Pb$ < 18.75), and they plot within the Pb isotope field for the alkali

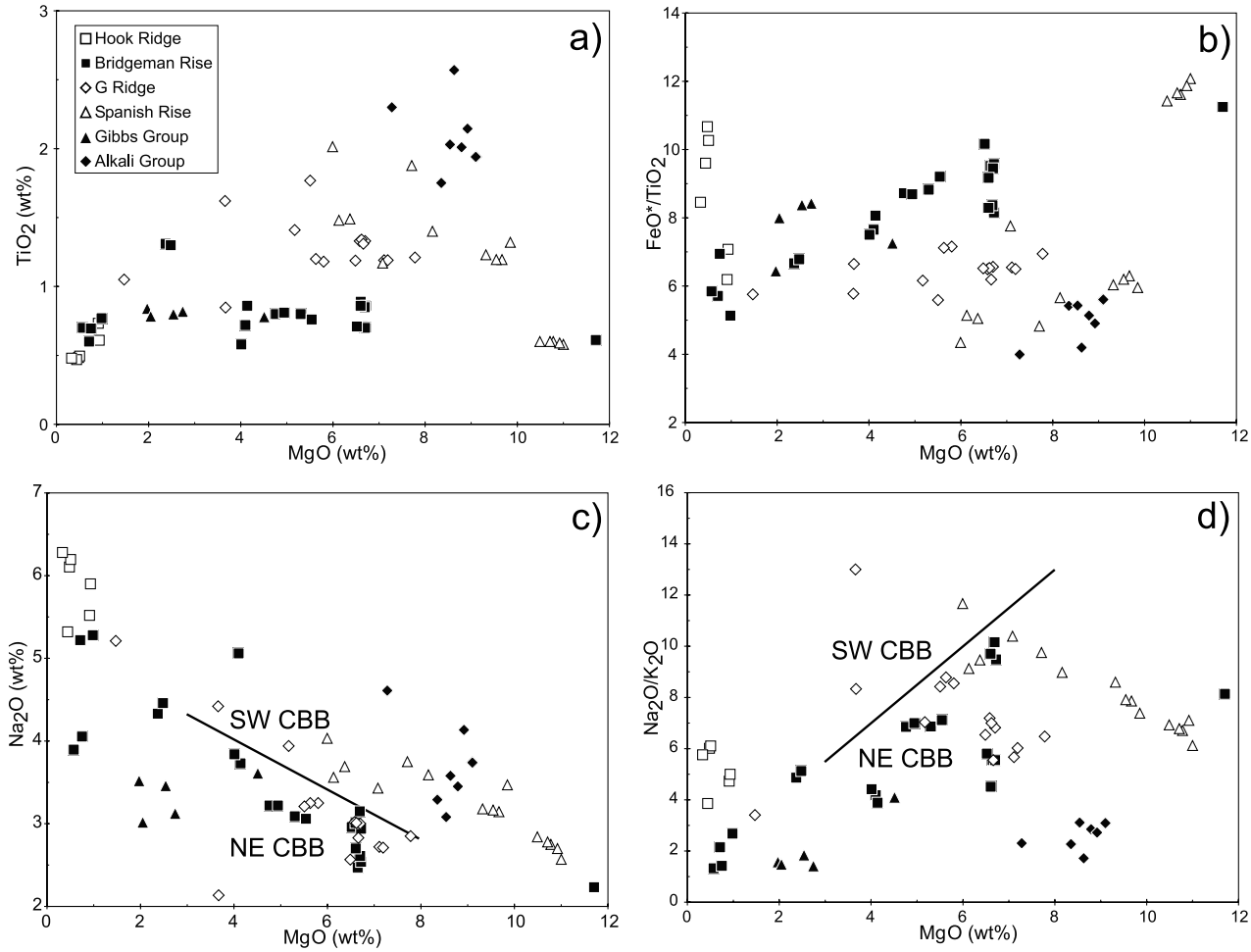

Figure 3. Plots of TiO_2, FeO^*/TiO_2, Na_2O, and Na_2O/K_2O versus MgO for the SO-155 lavas, demonstrating different values at MgO = 7 wt % and distinct fractionation trends for Bransfield Group lavas from different volcanic centers (Hook Ridge, Bridgeman Rise, G Ridge, Spanish Rise). Boundaries separating fields for lavas from the SW and NE central Bransfield Basin (SW CBB, NE CBB) are drawn from data of *Keller et al.* [2002].

basalts from James Ross Island, Seal Nunataks and Alexander Island (Figures 6b and 6c).

5. Discussion

5.1. Along-Axis Geochemical Variations

[24] A depth profile along the Bransfield Basin axis highlights the relatively smooth topography of the central subbasin relative to the deeper eastern subbasin and the location of the volcanic massifs (Figure 8a). Previous studies have found no systematic along-axis variations in lava geochemistry for the central Bransfield Basin [*Keller et al.*, 2002]. However, a complex and broadly symmetrical change is evident when those analyses are combined with the new analyses of eastern Bransfield Basin lavas. A general increase in LILE concentrations relative to the HFSE occurs across the central Bransfield Basin and reaches a maximum at Bridgeman Rise, as best shown by peak values of U/Nb and Rb/Nb (Figures 8b and 8c). Farther to the NE, U/Nb and Rb/Nb decline to low values for the Bransfield Primitive subgroup and other lavas outcropping on Spanish Rise. Similar trends are evident for Th/Nb, Pb/Yb, Ba/Nb and $^{87}Sr/^{86}Sr$, and are mirrored by variations in $^{143}Nd/^{144}Nd$ (Figure 8d). Thus the most MORB-like lavas occur in the central part of the central Bransfield Basin and at Spanish Rise in the eastern Bransfield Basin whereas the most arc-like lavas outcrop on Bridgeman Rise.

[25] Gibbs Group lavas form an exception to the general along-axis trend, as they have stronger LREE enrichment, higher LILE/HFSE values, and higher U/Nb than Bransfield Group lavas yet were recovered farther to the NE than Spanish Rise. These observations suggest Gibbs Group lavas are even more arc-like than lavas from Bridgeman Rise. The Alkali Group lavas, which lack any evidence of a slab-derived component, also form an exception to the general trend. We discuss the origin and relationships of these groups in the following sections.

5.2. Bransfield Group: Mantle Sources and Mixing Processes

[26] Bransfield Group lavas from both the central and eastern Bransfield Basin have elevated LILE concentrations relative to MORB, consistent with the addition of a slab-

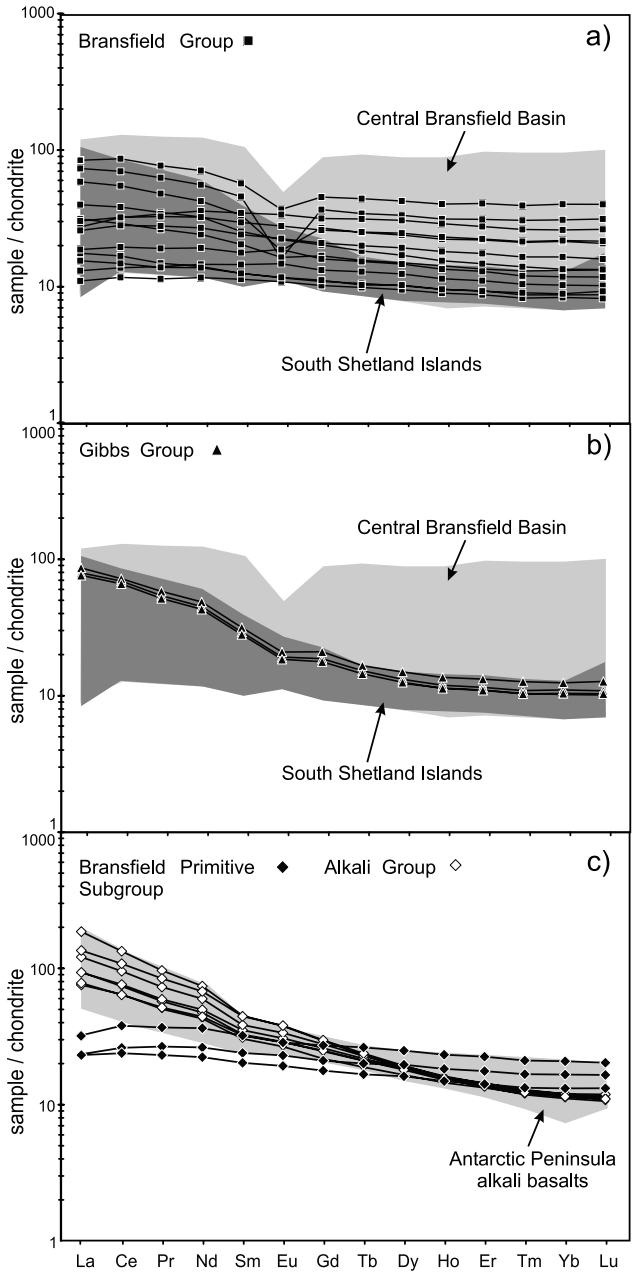

Figure 4. Chondrite-normalized REE patterns for (a) Bransfield Group lavas, (b) Gibbs Group lavas, and (c) Bransfield Primitive Subgroup and Alkali Group lavas. In Figures 4a and 4b, light shading denotes the range for central Bransfield Basin lavas and dark shading denotes that for lavas from the South Shetland Islands (data sources as for Figure 2). In Figure 4c, light shading gives the field for Antarctic Peninsula alkali basalts constructed from data of *Tarney et al.* [1982] and *Hole* [1990]. Chondrite composition is after *Sun and McDonough* [1989].

derived component to the sub-Bransfield mantle prior to partial melting. Part of this signature could also be generated by crustal assimilation during magma ascent, which can lead to enrichment in those elements hosted by the more fusible components of the crust. Changes in the ratios of strongly incompatible elements and Sr, Nd and Pb isotope composition with increasing fractionation are a hallmark of crustal assimilation [e.g., *Graham and Hackett*, 1987]. Such changes may occur for some Bridgeman Rise lavas, where a decrease in MgO from 12 to 1 wt % is accompanied by a general decrease in Ba/Rb from 9 to 5 and in Zr/Rb from 8 to 2. However, other incompatible element ratios show no changes (e.g., Rb/Cs), and there is no correlation between Sr, Nd or Pb isotope composition with any fractionation index. Lavas from G Ridge and Spanish Rise show no trend with fractionation indices, whereas rhyodacite from Hook Ridge (the most fractionated lava in Bransfield Group) has the same Ba/Rb as the most primitive Bridgeman Rise lava. Therefore any role for crustal assimilation was probably minor and insignificant except beneath Bridgeman Rise.

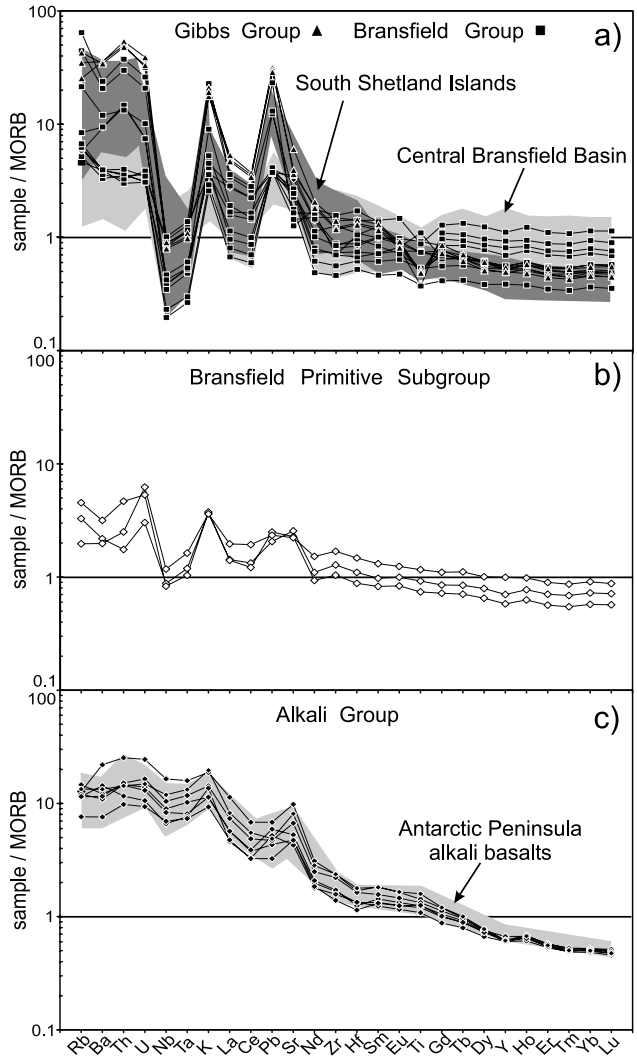

Figure 5. MORB-normalized incompatible element plots for (a) Bransfield and Gibbs Group lavas, (b) Bransfield Primitive Subgroup lavas, and (c) Alkali Group lavas. In Figure 5a, light shading denotes the range for central Bransfield Basin lavas and dark shading denotes that for lavas from the South Shetland Islands (data sources as for Figure 2). In Figure 5c, light shading denotes the range for Antarctic Peninsula alkali basalts (data sources as for Figure 4). NMORB composition is after *Hofmann* [1988].

[27] Variations in strongly incompatible element ratios and Sr, Nd and Pb isotope compositions among Bransfield Group lavas are instead attributed to changes in the magnitude of a slab-derived component fluxing the sub-Bransfield mantle. The Bransfield Primitive subgroup has the least enrichment in LILE relative to both the HREE and MORB, and is further characterized by HREE, Nb and Ta concentrations comparable to those of MORB (Figure 5b). These lavas also have nonradiogenic Sr and Nd isotope compositions that are near the midrange of Sr-Nd isotope compositions for Pacific and South Atlantic MORB (Figure 6). Nevertheless, values of Ce/Pb (Figure 9a) and $(Rb/Yb)_{MORB}$ in the range of 12–20 and 2–8, respectively, still imply the addition of a significant slab-derived component to the mantle source of these lavas. Other Bransfield Group and central Bransfield Basin lavas form an array extending to more radiogenic Sr–Nd compositions commensurate with their higher degrees of LILE enrichment relative to the HREE and MORB. This array is modeled as a mixing curve between a mantle end-member whose Sr and Nd isotopic composition is comparable to Pacific MORB and a slab-derived component (Figure 6a). For Pb, a mantle end-member composition with $^{207}Pb/^{204}Pb$ and $^{208}Pb/^{204}Pb$ similar to Pacific MORB is indicated by an extrapolation of the Bransfield Group array to values of Ce/Pb characteristic of MORB (Figure 9a; Ce/Pb ~ 25 [*Hofmann et al.*, 1986]). Low Pb isotope ratios are also required if the same mantle end-member featured in the genesis of the South Shetland arc lavas (Figures 6b, 6c, and 7).

[28] The slab-derived component is characterized by high concentrations of the fluid-mobile LILE, very low Ce/Pb ~ 1 and high Ba/Nb >200 (Figure 9). Strong fractionation of Ba from Nb implies this component was probably added as a hydrous fluid rather than a sediment melt, as fluids fractionate these elements much more efficiently than melts [*Johnson and Plank*, 1999]. For example, a 1% sediment fluid has a Ba/Nb of ~350 compared to a Ba/Nb of ~100 for a 5% sediment melt (Figure 9b). We suggest that the slab component is dominated by a contribution from subducting sediment rather than altered oceanic crust, as it must have high $^{87}Sr/^{86}Sr$ and Pb isotope ratios combined with low $^{143}Nd/^{144}Nd$ (<0.5128; Figure 9b). A similar conclusion was reached by *Keller et al.* [2002], although their preferred model featured bulk mixing of metalliferous sediments with a very depleted mantle composition. In contrast, we propose a mantle end-member with relatively radiogenic Pb isotope composition fluxed by a hydrous fluid derived predominantly from the subducting sediment. The slab-derived composition used in our model provides a good fit to the Bransfield Group array and has Sr, Nd and Pb isotope compositions and concentrations based on sediment analy-

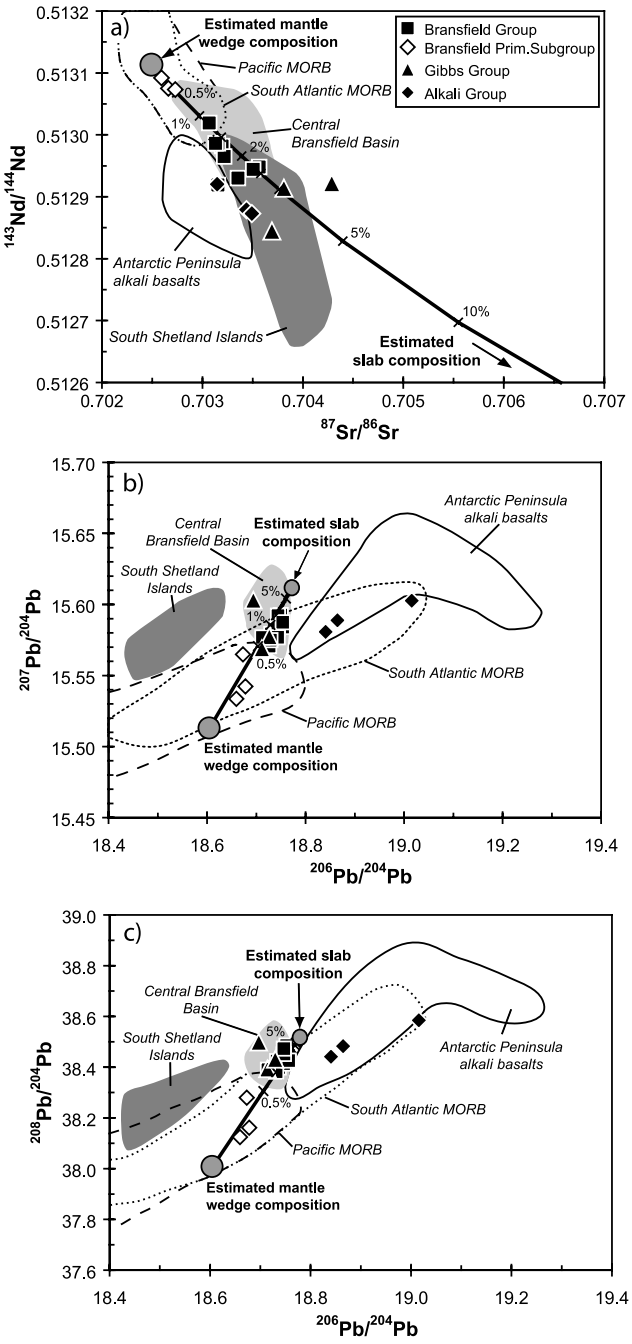

Figure 6. (a) Sr-Nd and (b) and (c) Pb-Pb isotope plots for Bransfield Basin lavas. Also shown are fields for lavas from the central Bransfield Basin (light shading) and South Shetland Islands (dark shading), Antarctic Peninsula alkali basalts, and Pacific and South Atlantic MORB. Data sources are as for Figures 2 and 4, with additional data from *Hanan et al.* [1986], *Birkenmajer et al.* [1991], *Bach et al.* [1994], *Mahoney et al.* [1994], *Klein and Karsten* [1995], *Bach et al.* [1996], *Fontignie and Schilling* [1996], *Castillo et al.* [1998], *Guangfu et al.* [1997], and *Vlastélic et al.* [1999]. Solid black curves with ticks model mixing between an inferred mantle wedge composition similar to Pacific MORB ($^{87}Sr/^{86}Sr = 0.7025$, $^{143}Nd/^{144}Nd = 0.51311$, $^{206}Pb/^{204}Pb = 18.6$, $^{207}Pb/^{204}Pb = 15.51$, $^{208}Pb/^{204}Pb = 38$, 20 ppm Sr, 1.6 ppm Nd, and 0.065 ppm Pb). For Pb, this wedge composition was chosen from an extrapolation of the Bransfield Group array to high Ce/Pb values characteristic of MORB (Figure 9a). The composition of the slab end-member was estimated from analyses of nearby South Atlantic sediments reported by *Ben Othman et al.* [1989] and *Walter et al.* [2000] ($^{87}Sr/^{86}Sr = 0.7092$, $^{143}Nd/^{144}Nd = 0.5124$, $^{206}Pb/^{204}Pb = 18.77$, $^{207}Pb/^{204}Pb = 15.61$, $^{208}Pb/^{204}Pb = 38.5$, 150 ppm Sr, 20 ppm Nd, and 20 ppm Pb). See text for further details.

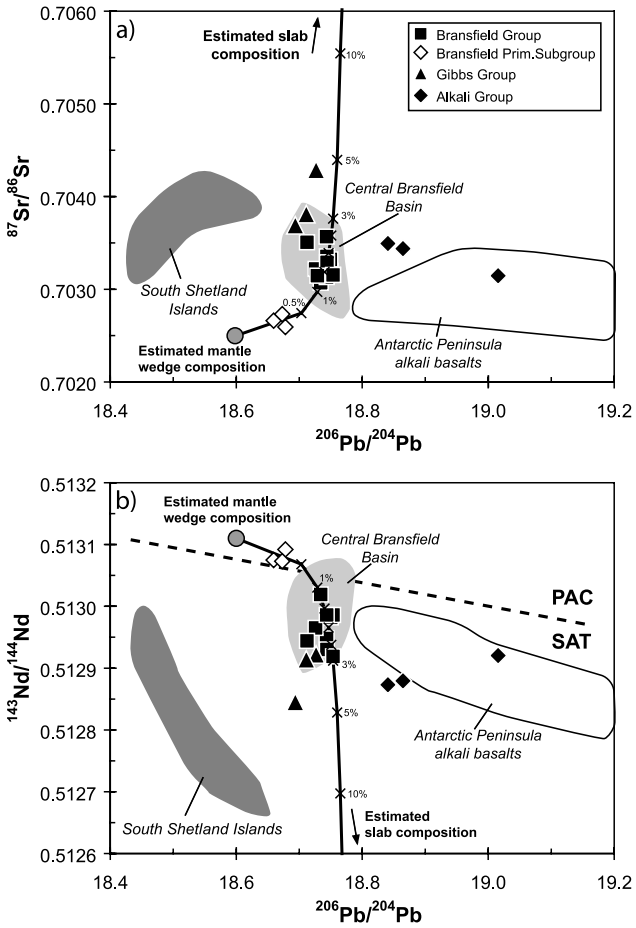

Figure 7. Plots of $^{87}Sr/^{86}Sr$ and $^{143}Nd/^{144}Nd$ versus $^{206}Pb/^{204}Pb$ for Bransfield Basin lavas. Also shown are fields for lavas from the central Bransfield Basin (light shading), South Shetland Islands (dark shading), and Antarctic Peninsula alkali basalts. Data sources and model end-member compositions are as for Figure 6. The dashed line discriminating between Pacific (PAC) and South Atlantic (SAT) MORB is taken from *Pearce et al.* [2001]). See text for further details.

ses from the South Atlantic and Bellingshausen Sea (Figures 6 and 7) [*Ben Othman et al.*, 1989; *Walter et al.*, 2000]. Mixing curves calculated for the chosen mantle and slab-derived compositions indicate the Bransfield Primitive subgroup lavas can be generated by adding ~0.5% of the slab-derived fluid to the mantle end-member, increasing to ~3% for the most radiogenic Bransfield Group lavas (Figures 6, 7, and 9).

5.3. Gibbs Rise: Relic of the South Shetland Arc?

[29] Gibbs Group lavas were recovered exclusively from the escarpment on Gibbs Rise, which has the morphology of a bisected cone whose NW half has been removed by faulting. The lavas were more weathered than those from other stations in the eastern Bransfield Basin, many were hydrothermally altered (chloritized and silicified), and dolerite blocks were also present in the dredge haul. Taken together, this suggests that Gibbs Group lavas represent a section through an extinct volcano and that they significantly predate the mostly fresh to weakly weathered lavas composing Bransfield Group. Gibbs Group lavas are strongly plagioclase-phyric, a characteristic typical of arc lavas elsewhere but one that stands in marked contrast to the sparsely phyric (<5% total phenocrysts) nature of most Bransfield Group lavas [this study; *Keller et al.*, 2002]. They also have the greatest degree of LILE enrichment relative to both the HREE and MORB, especially for K and Pb, although there is some overlap with the most LILE-enriched Bransfield Group lavas (Figure 5a). The greater LILE enrichment of Gibbs Group lavas is matched by their more radiogenic Sr and Nd isotope compositions, which plot closer to the inferred slab-derived end-member than those of Bransfield Group lavas (Figures 6, 7, and 9).

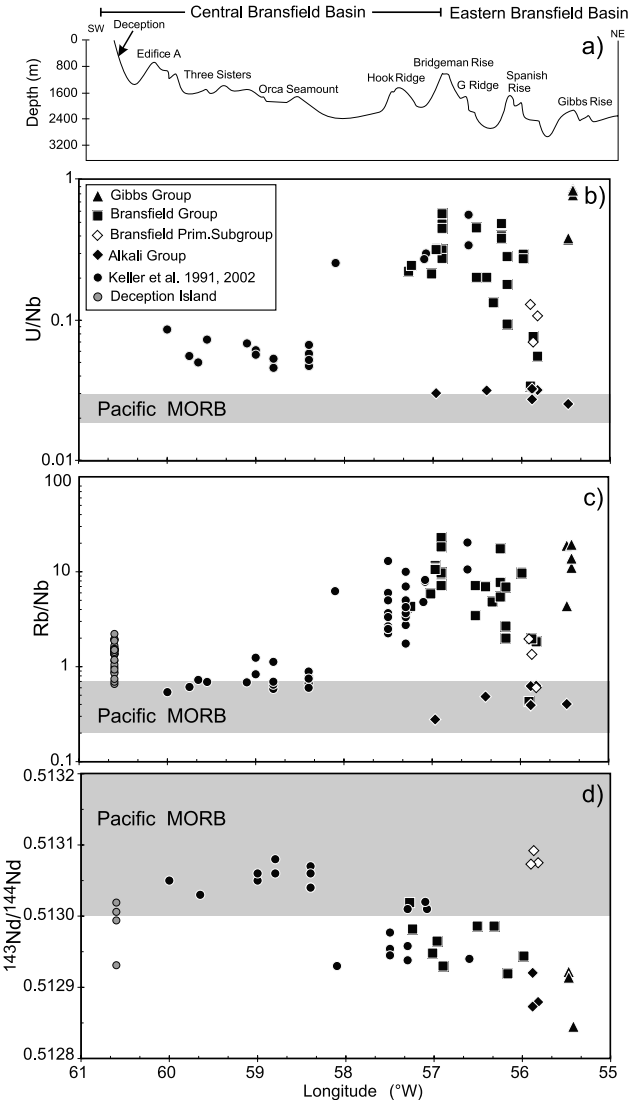

Figure 8. Variation along the Bransfield Basin axis of (a) water depth, with bathymetry from *Gràcia et al.* [1997] and a vertical exaggeration of 20, (b) U/Nb, (c) Rb/Nb, and (d) $^{143}Nd/^{144}Nd$ isotope values. Data for central Bransfield Basin lavas from *Keller et al.* [1991, 2002] and for Deception Island lavas are as given in Figure 2. Shaded fields represent Pacific MORB (data sources as for Figure 6).

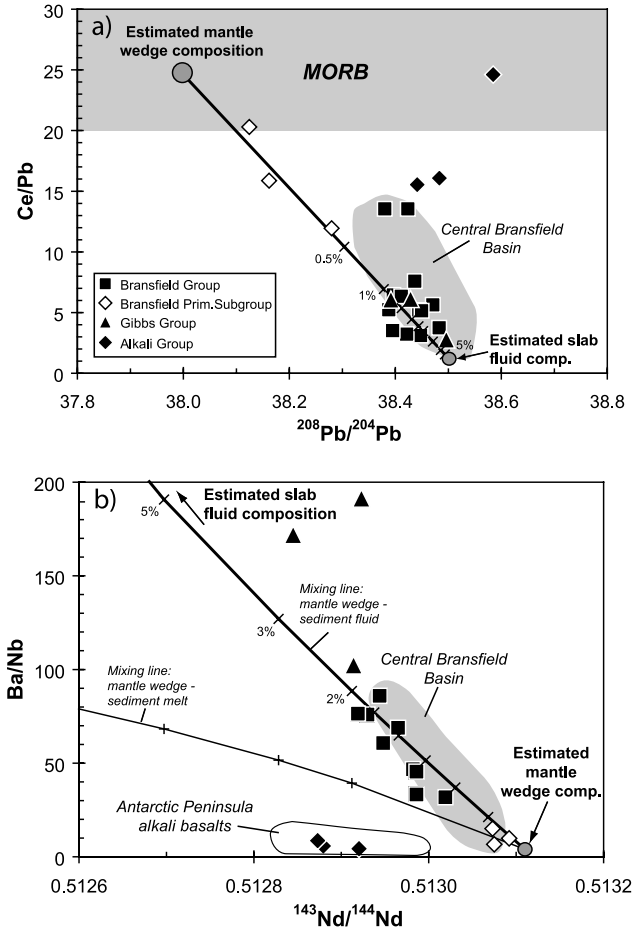

Figure 9. Plots of (a) Ce/Pb versus $^{208}Pb/^{204}Pb$, demonstrating that Bransfield Group and central Bransfield Basin lavas can be modeled by adding up to 5% of a slab-derived component to the sub-Bransfield mantle (MORB field from *Hofmann et al.* [1986]; end-members as in Figure 6, and 1.6 ppm Ce in mantle wedge and 25 ppm Ce in estimated slab component), and (b) Ba/Nb versus $^{143}Nd/^{144}Nd$, highlighting the very different composition of Alkali Group lavas which overlap with other Antarctic Peninsula alkali basalts (data sources and Nd isotopic end-member compositions as for Figure 6). Mixing lines were calculated using a mantle wedge end-member with 1.4 ppm Ba and 0.35 ppm Nb, sediment-derived fluid with 1275 ppm Ba and 3.6 ppm Nb, and a sediment-derived melt with 667 ppm Ba and 6.8 ppm Nb (see Figure 6 for isotope end-member compositions). Trace element concentrations for the sediment-derived fluid and melt are based on the work by *Plank and Langmuir* [1998] with Kd from *Johnson and Plank* [1999]. See text for further details.

[30] The evidence of greater age coupled with the most arc-like composition leads us to suspect Gibbs Rise is the remnant of a South Shetland arc volcano that partly collapsed as Bransfield Basin opened. An important corollary is that other South Shetland arc volcanoes may have suffered a similar fate. Therefore the paucity of post-20 Ma volcanism along the South Shetland Islands in the compilation of *Smellie et al.* [1984] could be explained by the post-20 Ma arc being located farther to the SE near the present axis of Bransfield Basin and undergoing subsidence as Bransfield Basin opened. This is consistent with seismic refraction profiles across the central Bransfield Basin, which reveal 0.5–1.5 km of sediment overlying basement interpreted as extended arc crust with seismic velocities of 3.5–6.5 km/s from 3–7 km depth increasing to 6.5–7.1 km/s from 7 km depth to the Moho [*Barker and Austin*, 1998; *Barker et al.*, 2003; *Christeson et al.*, 2003]. However, Gibbs Group lavas have higher $^{206}Pb/^{204}Pb$ relative to $^{207}Pb/^{204}Pb$ and $^{208}Pb/^{204}Pb$ than lavas from the South Shetland Islands (Figures 6 and 7). Therefore, if our interpretation of Gibbs Rise as a relic South Shetland arc volcano is correct, a significant change occurred in the Pb isotope composition of the slab-derived component between the last eruptions on the South Shetland Islands at ~20 Ma and volcanism at Gibbs Rise.

5.4. Alkali Group: Slab Window Versus Edge Flow

[31] The recovery of a large haul of fresh alkali basalt from station 26DR on Spanish Rise, and a few boulders at four other stations in the eastern Bransfield Basin, was unexpected. Alkaline lavas were erupted on James Ross Island and at Seal Nunataks between 7.1 and <1 Ma, and a predominantly older group were emplaced farther south on Alexander Island between 15 and <1 Ma (Figure 1a) [*Hole*, 1988, 1990; *Hole et al.*, 1991; *Smellie*, 1999]. The southern Alexander Island alkali basalts are the most voluminous. Their origin has been attributed to the opening of a slab window beneath the Antarctic Peninsula since 54 Ma following the progressive elimination of Antarctic-Phoenix spreading axis segments from SW to NE at the South Sandwich Trench [*Hole et al.*, 1991, 1995; *Barker and Austin*, 1998]. Localized upwellings of fresh asthenospheric mantle in the slab window led to decompression melting beginning in the garnet stability field and ultimately to eruption of the alkali basalts. All but a few Alexander Island alkali basalts lack any evidence of either a slab-derived component or interaction with crust in their genesis, and their eruption took place at time intervals as much as 30 Myr after initial window formation [*Hole et al.*, 1995].

[32] A different mechanism is required to generate the alkaline lavas recovered by us from Spanish Rise and those erupted on James Ross Island. These sites are too far north to be related to the southern slab window if, as envisaged by *Hole et al.* [1995] and *Barker and Austin* [1998], an intact slab persists beneath Bransfield Basin to the NW of the Hero Fracture Zone. The alkaline lavas from both Spanish Rise and James Ross Island lack any trace of a slab-related component. Therefore their genesis must also involve the upwelling and decompression melting of fresh asthenospheric mantle that has bypassed or avoided contact with subduction-modified lithosphere. One possible mechanism is slow roll-back at the South Shetland Trench [*Barker and Austin*, 1998]. The age of the subducting slab increases to the NE, which may lead to faster trench roll-back and induced SW directed mantle flow above the NE termination of the slab at the Shackleton Fracture Zone. This model predicts that eruptions of alkali basalt may commence in the eastern Bransfield Basin and later from sites farther to the SW. Significantly, Spanish Rise is the easternmost site of recent volcanism. Similar models of induced mantle flow around the edges of the slab subducting beneath the South

Sandwich arc have been proposed to explain the presence of Bouvet mantle plume material beneath the northernmost and southernmost segments of the back-arc East Scotia Ridge [*Leat et al.*, 2000; *Fretzdorff et al.*, 2002].

5.5. Is Bransfield Basin a Back-Arc Basin?

[33] Subduction of the Phoenix Plate at the South Shetland Trench slowed, and may have stopped, at 3.3 Ma when spreading ceased on the Antarctic-Phoenix Ridge [*Larter and Barker*, 1991; *Livermore et al.*, 2000]. Evidence for continued subduction is equivocal. No well-defined Wadati-Benioff zone extends from the South Shetland Trench beneath the South Shetland Islands and Bransfield Basin [*Pelayo and Wiens*, 1989], and few post-20 Ma lavas have been identified along the South Shetland arc [*Smellie et al.*, 1984]. Nevertheless, the South Shetland Trench retains the morphology of an active subduction zone [*Maldonado et al.*, 1994; *Jabaloy et al.*, 2003], and earthquake activity persists to ~65 km depth with focal mechanisms consistent with underthrusting [*Robertson Maurice et al.*, 2003]. Against this background, two general tectonic models have been proposed to explain post-3.3 Ma extension in the Bransfield Basin: (1) slow subduction at the South Shetland Trench coupled with no spreading at the Antarctic-Phoenix Plate may allow trench roll-back, which in turn generates extension across the Bransfield Basin [*Lawver et al.*, 1995; *Gràcia et al.*, 1996; *Barker and Austin*, 1998; *Barker et al.*, 2003; *Robertson Maurice et al.*, 2003], and (2) sinistral transcurrent movement between the Antarctic and Scotia Plates along the South Scotia Ridge fault may have propagated westward past the Shackleton Fracture Zone when subduction ceased, resulting in a transtensional environment for Bransfield Basin and compression in the South Shetland Islands [*González-Casado et al.*, 2000].

[34] These models predict different styles of magmatism in Bransfield Basin. If subduction continues, then the aseismic character of the subducting slab beneath ~65 km depth is best attributed to a hot slab whose temperature is in excess of 550°C at 65 km depth as a consequence of slow subduction (~1 cm/yr) of youthful oceanic lithosphere (14–23 Ma) [*Robertson Maurice et al.*, 2003]. Such conditions should favor partial melting of the slab under water-saturated conditions with residual garnet but not plagioclase. In consequence, the melt is expected to have adakitic affinities with high Sr/Y (>22, typically 50–80) and strong HREE depletion [*Drummond and Defant*, 1990; *Drummond et al.*, 1996]. This contrasts with the more general situation where a fluid flux is released into the mantle wedge from a comparatively cold slab [e.g., *Pearce and Peate*, 1995]. Although Bransfield Group lavas have a wide range in Sr and Y concentrations (62–433 ppm, excluding one outlier at 705 ppm, and 10–66 ppm respectively), Sr/Y does not exceed 22 except for the single outlier. Furthermore, their chondrite-normalized REE patterns are only weakly LREE-enriched with $(La/Yb)_N = 1.1–4.2$ (Figure 4). No Bransfield Group lavas can be classified as adakite, nor do they show any evidence for an adakitic component in their source.

[35] Numerous other features of Bransfield Basin magmatism are also not as expected from the continued subduction model. If subduction persists, then so should fluxing of the sub-Bransfield mantle by a slab-derived fluid. Gibbs Group lavas have the greatest slab-derived component of any Bransfield lavas but are significantly older than Bransfield Group lavas and come from a relic volcanic massif interpreted as part of the former South Shetland arc. Thus the slab-derived component in Bransfield lavas has decreased with time from Gibbs Group (equals South Shetland arc) to the more recent Bransfield Group lavas and reaches a minimum for lavas of the Bransfield Primitive subgroup, which are isotopically similar to Pacific MORB. Bransfield Group lavas also require considerable source heterogeneity (variable $Ti_{7.0}$ and $Na_{7.0}$), rather than the more uniform source that might be expected from extensive fluid fluxing of the mantle wedge above a subducting slab.

[36] It might be argued that changes in the slab-derived component with time and mantle heterogeneity are found at other active back-arc basins, and these features do characterize the Lau Basin and Mariana Trough [e.g., *Stern et al.*, 1990; *Hawkins*, 1995]. However, those back-arc systems also feature robust arc volcanism, well-defined subducting slabs, and increased back-arc volcanism as the slab-derived component dwindles and the system evolves from rifting to crustal accretion at a well-defined spreading center. For Bransfield Basin there is no active arc, no seismically active slab beneath 65 km depth, and volcanism rapidly diminishes in the eastern Bransfield Basin as the slab-derived component declines and the crust thins. Evidence of mantle heterogeneity and a dwindling slab-derived component in the sub-Bransfield mantle is further supported by the presence of young Alkali Group lavas in the eastern Bransfield Basin. They show no trace element or isotopic evidence of any slab-derived component. Therefore complete removal of the sub-South Shetland arc mantle from their source region prior to melt generation is required.

[37] It has been proposed that Bransfield Basin is at an advanced stage of back-arc basin development, and that a change may occur from rifting in the eastern Bransfield Basin to incipient spreading in the wider central Bransfield Basin [*Gràcia et al.*, 1996]. This model found support in the relatively MORB-like lavas erupted in the central Bransfield Basin compared to the more arc-like lavas from Bridgeman Rise [*Keller et al.*, 2002]. However, recent studies show that the crustal thickness consistently decreases to the NE and becomes thinner beneath the eastern Bransfield Basin [*Christeson et al.*, 2003]. This is accompanied by the eruption of the most MORB-like lavas from Spanish Rise. Farther to the NE, we found no evidence of recent volcanism in the widest part of the eastern Bransfield Basin, and much of Spanish Rise and G Ridge have not been resurfaced in recent times. The rough bathymetry of the deep eastern Bransfield Basin reflects tectonism and slumping of the basin margins. Extension in the NE part of the eastern subbasin is amagmatic.

[38] How can the paucity of volcanism in the eastern Bransfield Basin and dwindling slab-derived component in the Bransfield Basin lavas with time be reconciled with the tectonic environment? We contend that these observations are more consistent with the alternative model of basin opening in response to transtension induced by westward propagation of the South Scotia Ridge fault [*González-Casado et al.*, 2000]. We propose that the South Shetland arc became extinct and no further fluid was released from the slab into the sub-Bransfield mantle after subduction drastically slowed (or ceased) at 3.3 Ma. Subsequent crustal

thinning during basin opening, propagating from the NE to SW, would then permit passive upwelling of the mantle. Subduction-modified mantle will melt more readily on account of its greater H_2O content. In the absence of further fluid input from the now stalled or absent slab, magmatism should diminish with time as the subduction component is progressively melted out of the sub-Bransfield mantle. An important feature of this model is that a pulse of magmatism will follow the SW directed propagation of the South Scotia Ridge fault. This is similar to the observed distribution of volcanism in the Bransfield Basin, which is presently concentrated in the central Bransfield Basin and diminishes to both the NE and SW. In particular, the model predicts the relatively amagmatic character of the eastern Bransfield Basin and occurrence of lavas with the least slab-derived contribution at the most easterly volcanic center (Spanish Rise).

[39] In conclusion, the distribution and composition of lavas recovered from the Bransfield Basin provide no support for models invoking continued trench roll-back and slow subduction as the driving force for basin opening. Our results are consistent with an alternative model featuring basin development as a consequence of SW directed propagation of the South Scotia Ridge fault since 3 Ma. In any event, there is no active volcanic arc. Therefore Bransfield Basin should not be classified as a back-arc basin. It is properly designated an actively extending marginal basin.

[40] **Acknowledgments.** We thank Dieter Garbe-Schönberg, Folkmar Hauff and Silke Vetter for assistance with the ICP-MS analyses and isotope work. We also thank Peter Herzig (Chief Scientist), Hartmut Andresen (Captain), and the crew and shipboard scientific party of FS *Sonne* cruise SO-155 for their expertise and help during the sampling program. Constructive reviews by Julian Pearce and Alison Shaw, together with editorial comments by Bruce Nelson, are gratefully acknowledged and led to an improved manuscript. This work was funded by the Bundesministerium für Bildung und Forschung (BMBF grant 03GO155C). Roger Hékinian acknowledges financial support from the Alexander von Humboldt Foundation. Randy Keller's participation was supported by the NSF Office of Polar Programs.

References

Bach, W., E. Hegner, J. Erzinger, and M. Satir (1994), Chemical and isotopic variations along the superfast spreading East Pacific Rise from 6 to 30°S, *Contrib. Mineral. Petrol.*, *116*, 365–380.

Bach, W., J. Erzinger, L. Dosso, C. Bollinger, H. Bougault, J. Etoubleau, and J. Sauerwein (1996), Unusually large Nb-Ta depletions in north Chile ridge basalts at 36°50′ to 38°56′S: Major element, trace element, and isotopic data, *Earth Planet. Sci. Lett.*, *142*, 223–240.

Baker, P. E., I. McReath, M. R. Harvey, M. J. Roobol, and T. G. Davies (1975), The geology of the South Shetland Islands: V. Volcanic evolution of Deception Island, *Br. Antarct. Surv. Sci. Rep.*, *78*, 79pp.

Barker, D. H. N., and J. A. Austin Jr. (1998), Rift propagation, detachment faulting, and associated magmatism in Bransfield Strait, Antarctic, *J. Geophys. Res.*, *103*(B10), 24,017–24,043.

Barker, D. H. N., G. L. Christeson, J. A. J. Austin, and I. W. D. Dalziel (2003), Backarc basin evolution and cordilleran orogenesis: Insights from new ocean-bottom seismograph refraction profiling in Bransfield Strait, Antarctica, *Geology*, *31*, 107–110.

Barker, P. F. (1982), The Cenozoic subduction history of the Pacific margin of the Antarctic Peninsula: Ridge crest-trench interactions, *J. Geol. Soc. London*, *139*, 787–801.

Barker, P. F., I. W. D. Dalziel, and B. C. Storey (1991), Tectonic development of the Scotia arc region, in *The Geology of Antarctica*, edited by R. J. Tingey, pp. 215–248, Clarendon, Oxford, U.K.

Ben Othman, D., W. M. White, and J. Patchett (1989), The geochemistry of marine sediments, island arc magma genesis, and crust-mantle recycling, *Earth Planet. Sci. Lett.*, *94*, 1–21.

Birkenmajer, K., M. C. Delitala, W. Narebski, M. Nicoletti, and C. Petrucciani (1986), Geochronology and migration of Cretaceous through Tertiary plutonic centres, South Shetland Islands (West Antarctica): Subduction and hot spot magmatism, *Bull. Pol. Acad. Sci. Earth Sci.*, *34*, 243–255.

Birkenmajer, K., L. Francalanci, and A. Peccerillo (1991), Petrological and geochemical constraints on the genesis of Mesozoic-Cenozoic magmatism of King George Island, South Shetland Islands, Antarctica, *Antarct. Sci.*, *3*, 293–308.

Castillo, P. R., J. H. Natland, Y. Niu, and P. F. Lonsdale (1998), Sr, Nd and Pb isotopic variation along the Pacific-Antarctic rise crest, 53–57°S: Implications for the composition and dynamics of the South Pacific upper mantle, *Earth Planet. Sci. Lett.*, *154*, 109–125.

Christeson, G. L., D. H. N. Barker, J. A. Austin, and I. W. D. Dalziel (2003), Deep crustal structure of Bransfield Strait: Initiation of a back arc basin by rift reactivation and propagation, *J. Geophys. Res.*, *108*(B10), 2492, doi:10.1029/2003JB002468.

Dählmann, A., K. Wallmann, H. Sahling, G. Sarthou, G. Bohrmann, S. Petersen, C. S. Chin, and G. P. Klinkhammer (2001), Hot vents in an ice-cold ocean: Indications for phase seperation at the southernmost area of hydrothermal activity, Bransfield Strait, Antarctica, *Earth Planet. Sci. Lett.*, *193*, 381–394.

Dietrich, R., et al. (2001), ITRF coordinates and plate velocities from repeated GPS campaigns in Antarctica; an analysis based on different individual solutions, *J. Geod.*, *74*, 756–766.

Drummond, M. S., and M. J. Defant (1990), A model for trondhjemite-tonalite-dacite genesis and crustal growth via slab melting; Archean to modern comparisons, *J. Geophys. Res.*, *95*(B13), 21,503–21,521.

Drummond, M. S., M. J. Defant, and P. K. Kepezhinskas (1996), Petrogenesis of slab-derived trondhjemite-tonalite-dacite/adakite magmas, in *The Third Hutton Symposium on the Origin of Granites and Related Rocks*, edited by M. Brown et al., pp. 205–215, Geol. Soc. of Am., Boulder, Colo.

Fisk, M. R. (1990), Volcanism in the Bransfield Strait, Antarctica, *J. South Am. Earth Sci.*, *3*, 91–101.

Fontignie, D., and J.-G. Schilling (1996), Mantle heterogeneities beneath the South Atlantic: A Nd-Sr-Pb isotope study along the Mid-Atlantic Ridge (3°S–46°S), *Earth Planet. Sci. Lett.*, *142*, 209–221.

Fretzdorff, S., R. A. Livermore, C. W. Devey, P. T. Leat, and P. Stoffers (2002), Petrogenesis of the back-arc East Scotia Ridge, South Atlantic Ocean, *J. Petrol.*, *43*, 1435–1467.

Fryer, P., B. Taylor, C. H. Langmuir, and A. G. Hochstaedter (1990), Petrology and geochemistry of lavas from the Sumisu and Torishima backarc rifts, *Earth Planet. Sci. Lett.*, *100*, 161–178.

Gambôa, L. A. P., and P. R. Maldonado (1990), Geophysical investigations in the Bransfield Strait and in the Bellingshausen Sea, Antarctica, in *Antarctica as an Exploration Frontier: Hydrocarbon Potential, Geology, and Hazards*, edited by B. St. John, pp. 127–141, Am. Assoc. of Pet. Geol., Tulsa, Okla.

Garbe-Schönberg, C.-D. (1993), Simultaneous determination of thirty-seven trace elements in twenty-eight international rock standards by ICP-MS, *Geostand. Newsl.*, *17*, 81–97.

González-Casado, J. M., J. L. Giner-Roles, and J. López-Martinez (2000), Bransfield Basin, Antarctic Peninsula: Not a normal backarc basin, *Geology*, *28*, 1043–1046.

González-Ferrán, O. (1991), The Bransfield Rift and its active volcanism, in *Geological Evolution of Antarctica*, edited by M. R. A. Thompson, J. A. Crame, and J. W. Thomson, pp. 505–509, Cambridge Univ. Press, New York.

Govindaraju, K. (1994), Compilation of working values and sample-description for 383 geostandards, *Geostand. Newsl.*, *13*, 1–158.

Gràcia, E., M. Canals, M. Li Farran, M. J. Prieto, J. Sorribas, and GEBRA Team (1996), Morphostructure and evolution of the central and eastern Bransfield Basins (NW Antarctic Peninsula), *Mar. Geophys. Res.*, *18*, 429–448.

Gràcia, E., M. Canals, M. L. Farràn, J. Sorribas, and R. Pallàs (1997), Central and eastern Bransfield Basins (Antarctica) from high-resolution swath-bathymetry data, *Antarct. Sci.*, *9*, 168–180.

Graham, I. J., and W. R. Hackett (1987), Petrology of calc-alkaline lavas from Ruapehu Volcano and related vents, Taupo Volcanic Zone, New Zealand, *J. Petrol.*, *28*, 531–567.

Gribble, R. F., R. J. Stern, S. Newman, S. H. Bloomer, and T. O'Hearn (1998), Chemical and isotopic composition of lavas from the northern Mariana Trough: Implications for magmagenesis in back-arc basins, *J. Petrol.*, *39*, 125–154.

Guangfu, X., S. Weizhou, W. Dezi, and J. Qingmin (1997), Sr-Nd-Pb isotopes of Tertiary volcanics of King George Island, Antarctica, *Chin. Sci. Bull.*, *42*, 1913–1918.

Hanan, B. B., R. H. Kingsley, and J. G. Schilling (1986), Pb isotope evidence in the South Atlantic for migrating ridge-hotspot interactions, *Nature*, *322*, 137–144.

Hawkins, J. W. (1995) Evolution of the Lau Basin: Insights from ODP Leg 135, in *Active Margins and Marginal Basins of the Western Pacific*,

Geophys. Monogr. Ser., vol. 88, edited by B. Taylor and J. Natland, pp. 125–173, AGU, Washington, D. C.

Herzig, P., and Party of SO-155 (2001), Volcanism, Hydrothermal processes and faunal communities at shallow submarine volcanoes, Bransfield back-arc, Antarctica, *Cruise Rep. R/V Sonne Cruise SO-155*, 114 pp., Freiberg Univ. of Min. and Technol., Freiberg, Germany.

Hoernle, K. A., and G. R. Tilton (1991), Sr-Nd-Pb isotope data for Fuerteventura (Canary Islands) basal complex and subaerial volcanics: Applications to magma genesis and evolution, *Schweiz. Mineral. Petrogr. Mitt.*, *71*, 3–18.

Hofmann, A. W. (1988), Chemical differentiation of the Earth: The relationship between mantle, continental crust, and oceanic crust, *Earth Planet. Sci. Lett.*, *90*, 297–314.

Hofmann, A. W., K. P. Jochum, M. Seufert, and W. M. White (1986), Nb and Pb in oceanic basalts: New constraints on mantle evolution, *Earth Planet. Sci. Lett.*, *79*, 33–45.

Hole, M. J. (1988), Post-subduction alkaline volcanism along the Antarctic Peninsula, *J. Geol. Soc. London*, *145*, 985–988.

Hole, M. J. (1990), Geochemical evolution of Pliocene-Recent post-subduction alkalic basalts from Seal Nunataks, Antarctic Peninsula, *J. Volcanol. Geotherm. Res.*, *40*, 149–167.

Hole, M. J., R. J. Pankhurst, and A. D. Saunders (1991), Geochemical evolution of the Antarctic Peninsula magmatic arc: The importance of mantle-crust interactions during granitoid genesis, in *Geological Evolution of Antarctica*, edited by M. R. A. Thompson, J. A. Crame, and V. W. Thompson, pp. 369–375, Cambridge Univ. Press, New York.

Hole, M. J., P. D. Kempton, and I. L. Millar (1993), Trace-element and isotopic characteristics of small-degree melts of the asthenosphere: Evidence from the alkalic basalts of the Antarctic Peninsula, *Chem. Geol.*, *109*, 51–68.

Hole, M. J., A. D. Saunders, G. Rogers, and M. A. Sykes (1995), The relationship between alkaline magmatism, lithospheric extension and slab window formation along continental destructive plate margins, in *Volcanism Associated With Extension at Consuming Plate Margins*, edited by J. L. Smellie, *Geol. Soc. Spec. Publ.*, *80*, 265–285.

Jabaloy, A., et al. (2003), The transition from an active to a passive margin (SW end of the South Shetland Trench, Antarctic Peninsula), *Tectonophysics*, *366*, 55–81.

Jenner, G. A., H. P. Longerich, S. E. Jackson, and B. J. Fryer (1990), A powerful tool for high-precision trace element analysis in earth sciences: Evidence from analysis of selected U.S. G. S. reference samples, *Chem. Geol.*, *83*, 133–148.

Johnson, M. C., and T. Plank (1999), Dehydration and melting experiments constrain the fate of subducted sediments, *Geochem. Geophys. Geosyst.*, *1*, doi:10.1029/1999GC000014.

Keller, R. A., M. R. Fisk, W. M. White, and K. Birkenmajer (1991), Isotopic and trace element constraints on mixing and melting models of marginal basin volcanism, Bransfield Strait, Antarctica, *Earth Planet. Sci. Lett.*, *111*, 287–303.

Keller, R. A., M. R. Fisk, J. L. Smellie, J. A. Strelin, and L. A. Lawver (2002), Geochemistry of back arc basin volcanism in Bransfield Strait, Antarctica: Subducted contributions and along-axis variations, *J. Geophys. Res.*, *107*(B8), 2171, doi:10.1029/2001JB000444.

Klein, E. M., and J. L. Karsten (1995), Ocean-ridge basalts with convergent-margin geochemical affinities from the Chile Ridge, *Nature*, *374*, 52–57.

Klepeis, K. A., and L. A. Lawver (1996), Tectonics of the Antarctic-Scotia plate boundary near Elephant and Clarence Islands, West Antarctica, *J. Geophys. Res.*, *101*(B9), 20,211–20,231.

Klinkhammer, G. P., C. S. Chin, R. A. Keller, A. Dählmann, H. Sahling, G. Sarthou, S. Petersen, F. Smith, and C. Wilson (2001), Discovery of new hydrothermal vent sites in Bransfield Strait, Antarctica, *Earth Planet. Sci. Lett.*, *193*, 395–407.

Larter, R. D., and P. F. Barker (1991), Effects of ridge crest-trench interaction on Antarctic-Phoenix spreading: Forces on a young subducting plate, *J. Geophys. Res.*, *96*(B12), 19,583–19,607.

Lawver, L. A., R. A. Keller, M. R. Fisk, and J. A. Strelin (1995), Bransfield Strait, Antarctic Peninsula: Active extension behind a dead arc, in *Back-arc Basins: Tectonics and Magmatism*, edited by B. Taylor, pp. 315–342, Plenum, New York.

Lawver, L. A., B. J. Sloan, D. H. N. Barker, M. Ghidella, R. P. von Herzen, R. A. Keller, G. P. Klinkhammer, and C. S. Chin (1996), Distributed active extension in Bransfield Basin, Antarctic Peninsula: Evidence from multi-beam bathymetry, *GSA Today*, *6*, 1–6.

Leat, P. T., R. A. Livermore, I. L. Millar, and J. A. Pearce (2000), Magma supply in back-arc spreading centre segment E2, East Scotia Ridge, *J. Petrol.*, *41*, 845–866.

Livermore, R., et al. (2000), Autopsy on a dead spreading center: The Phoenix Ridge, Drake Passage, Antarctica, *Geology*, *28*, 607–610.

Mahoney, J. J., J. M. Sinton, M. D. Kurz, J. D. Macdougall, K. J. Spencer, and G. W. Lugmair (1994), Isotope and trace element characteristics of a super-fast spreading ridge: East Pacific Rise, 13–23°S, *Earth Planet. Sci. Lett.*, *121*, 173–193.

Maldonado, A., R. D. Larter, and F. Aldaya (1994), Forearc tectonic evolution of the South Shetland Margin, Antarctic Peninsula, *Tectonics*, *13*, 1345–1370.

Martinez, F., and B. Taylor (2003), Controls on back-arc crustal accretion: Insights from the Lau, Manus and Mariana basins, in *Intra-oceanic Subduction Systems: Tectonic and Magmatic Processes*, edited by R. D. Larter and P. T. Leat, *Geol. Soc. Spec. Publ.*, *219*, 19–54.

Pankhurst, R. J., and J. L. Smellie (1983), K-Ar geochronology of the South Shetland Islands, Lesser Antarctica: Apparent lateral migration of Jurassic to Quaternary island arc volcanism, *Earth Planet. Sci. Lett.*, *66*, 214–222.

Parson, L. M., and I. C. Wright (1996), The Lau-Havre-Taupo back-arc basin; a southward-propagating, multi-stage evolution from rifting to spreading, *Tectonophysics*, *263*, 1–22.

Pearce, J. A., and D. W. Peate (1995), Tectonic implications of the composition of volcanic arc magmas, *Annu. Rev. Earth Planet. Sci.*, *23*, 251–285.

Pearce, J. A., M. Ernewein, S. H. Bloomer, L. M. Parson, B. J. Murton, and L. E. Johnson (1995), Geochemistry of Lau basin volcanic rocks: Influence of ridge segmentation and arc proximity, in *Volcanism Associated With Extension at Consuming Plate Margins*, edited by J. L. Smellie, *Geol. Soc. Spec. Publ.*, *81*, 53–75.

Pearce, J. A., P. T. Leat, P. F. Barker, and I. L. Millar (2001), Geochemical tracing of Pacific-to-Atlantic upper-mantle flow through the Drake Passage, *Nature*, *410*, 457–461.

Peate, D. W., T. F. Kokfelt, C. J. Hawkesworth, P. W. van Calsteren, J. M. Hergt, and J. A. Pearce (2001), U-series isotope data on Lau Basin glasses: The role of subduction-related fluids during melt generation in back-arc basins, *J. Petrol.*, *42*, 1449–1470.

Peccerillo, A., and S. R. Taylor (1976), Geochemistry of Eocene calc-alkaline volcanic rocks from the Kastamonu area, northern Turkey, *Contrib. Mineral. Petrol.*, *58*, 63–81.

Pelayo, A. M., and D. A. Wiens (1989), Seismotectonics and relative plate motions in the Scotia Sea Region, *J. Geophys. Res.*, *94*(B6), 7293–7320.

Plank, T., and C. H. Langmuir (1998), The chemical composition of subducting sediment and its consequences for the crust and mantle, *Chem. Geol.*, *145*, 325–394.

Prieto, M. J., G. Ercilla, M. Canals, and M. de Batist (1999), Seismic stratigraphy of the central Bransfield Basin (NW Antarctic Peninsula): Interpretation of deposits and sedimentary processses in a glacio-marine environment, *Mar. Geol.*, *157*, 47–68.

Robertson Maurice, S. D., D. A. Wiens, P. J. Shore, E. Vera, and L. M. Dorman (2003), Seismicity and tectonics of the South Shetland Islands and Bransfield Strait from a regional broadband seismograph deployment, *J. Geophys. Res.*, *108*(B10), 2461, doi:10.1029/2003JB002416.

Saunders, A. D., and J. Tarney (1984), Geochemical characteristics of basaltic volcanism within back-arc basins, in *Marginal Basin Geology: Volcanic and Associated Sedimentary and Tectonic Processes in Modern and Ancient Marginal Basins*, edited by B. P. Kokelaar and M. F. Howells, *Geol. Soc. Spec. Publ.*, *16*, 59–76.

Sinton, J. M., L. L. Ford, B. Chappell, and M. T. McCulloch (2003), Magma genesis and mantle heterogeneity in the Manus back-arc basin, Papua New Guinea, *J. Petrol.*, *44*, 159–195.

Smellie, J. L. (1999), Lithostratigraphy of Miocene-Recent, alkaline volcanic fields in the Antarctic Peninsula and eastern Ellsworth Land, *Antarct. Sci.*, *11*, 362–378.

Smellie, J. L., R. J. Pankhurst, M. R. A. Thomson, and R. E. S. Davies (1984), The geology of the South Shetland Islands: VI. Stratigraphy, geochemistry and evolution, *Br. Antarct. Surv. Sci. Rep.*, *87*, 85 pp.

Smellie, J. L., R. J. Pankhurst, M. J. Hole, and J. W. Thomson (1988), Age, distribution and eruptive conditions of late Cenozoic alkaline volcanism in the Antarctic Peninsula and eastern Ellsworth Land; review, *Br. Antarct. Surv. Bull.*, *80*, 21–49.

Smellie, J. L., A. Hofstetter, and G. Troll (1992), Fluorine and boron geochemistry of an ensialic marginal basin volcano: Deception Island, Bransfield Strait, Antarctica, *J. Volcanol. Geotherm. Res.*, *49*, 255–267.

Somoza, L., J. Martinez-Frias, J. L. Smellie, J. Rey, and A. Maestro (2004), Evidence for hydrothermal venting and sediment volcanism discharged after recent short-lived volcanic eruptions at Deception Island, Bransfield Strait, Antarctica, *Mar. Geol.*, *203*, 119–140.

Stern, R. J., P.-N. Lin, J. D. Morris, M. C. Jackson, P. Fryer, S. H. Bloomer, and E. Ito (1990), Enriched back-arc basin basalts from the northern Mariana Trough: Implications for the magmatic evolution of back-arc basins, *Earth Planet. Sci. Lett.*, *100*, 210–225.

Sun, S.-S., and W. F. McDonough (1989), Chemical and isotopic systematics of oceanic basalts: Implications for mantle composition and pro-

cesses, in *Magmatism in the Ocean Basins*, edited by A. D. Saunders and M. J. Norry, *Geol. Soc. Spec. Publ.*, *42*, 313–345.

Tarney, J., S. D. Weaver, A. D. Saunders, R. J. Pankhurst, and P. F. Barker (1982), Volcanic evolution of the northern Antarctic Peninsula and the Scotia arc, in *Andesites*, edited by R. S. Thorpe, pp. 371–413, John Wiley, Hoboken, N. J.

Taylor, B., and F. Martinez (2003), Back-arc basin basalt systematics, *Earth Planet. Sci. Lett.*, *210*, 481–497.

Thorkelson, D. J. (1996), Subduction of diverging plates and the principles of slab window formation, *Tectonophysics*, *255*, 47–63.

Todt, W., R. A. Cliff, A. Hanser, and A. W. Hofmann (1996), Evaluation of a ^{202}Pb-^{205}Pb double spike for high precision lead isotope analyses, in *Earth Processes: Reading the Isotopic Code*, *Geophys. Monogr. Ser.*, vol. 95, edited by A. Basu and S. Hart, pp. 429–437, AGU, Washington, D. C.

Vlastélic, I., D. Aslanian, L. Dosso, H. Bougault, J. L. Olivet, and L. Géli (1999), Large-scale chemical and thermal division of the Pacific mantle, *Nature*, *399*, 345–350.

Walter, H. J., E. Hegner, B. Diekmann, G. Kuhn, and M. M. Rutgers van der Loeff (2000), Provenance and transport of terrigenous sediment in the South Atlantic Ocean and their relations to glacial and interglacial cycles: Nd and Sr isotopic evidence, *Geochim. Cosmochim. Acta*, *64*, 3813–3827.

Weaver, S. D., A. D. Saunders, R. J. Pankhurst, and J. Tarney (1979), A geochemical study of magmatism associated with the initial stages of back-arc spreading: The Quaternary volcanics of Bransfield Strait from South Shetland Islands, *Contrib. Mineral. Petrol.*, *68*, 151–169.

L. Franz, Institut für Mineralogie, TU Bergakademie Freiberg, Brennhausgasse 14, D-09596 Freiberg, Germany.

S. Fretzdorff, K. M. Haase, R. Hékinian, P. Stoffers, and T. J. Worthington, Institut für Geowissenschaften, Abteilung Geochemie, Christian-Albrechts-Universität zu Kiel, Olshausenstrasse 40, D-24118 Kiel, Germany. (sf@gpi.uni-kiel.de)

R. A. Keller, College of Oceanic and Atmospheric Sciences, Oregon State University, 104 COAS Admin Building, Corvallis, OR 97331-5503, USA.